Lightning Assimilation in the WRF-model (Version 4.1.1): Technique Updates and Assessment of the Applications from Regional to Hemispheric Scales

Daiwen Kang[1*], Nicholas K. Heath[2#], Robert C. Gilliam[1], Tanya L. Spero[1], and Jonathan E. Pleim[1]

[1] Center for Environmental Measurement and Modeling, Office of Research and Development, U.S. Environmental Protection Agency, Research Triangle Park, NC 27711, U.S.A.

[2] Air Quality and Atmospheric Composition, Atmospheric and Environmental Research, Lexington, MA 02421, U.S.A.

*Correspondence: kang.daiwen@epa.gov

[#]Currently working as an independent consultant

Abstract: The lightning assimilation (LTA) technique in the Kain-Fritsch convective parameterization in the WRF model has been updated and applied to continental and hemispheric simulations using lightning flash data obtained from the National Lightning Detection Network (NLDN) and the World Wide Lightning Location Network (WWLLN), respectively. The impact of different values for cumulus parameters associated with the Kain-Fritsch scheme on simulations with and without LTA were evaluated for both the continental and the hemispheric simulations. Comparisons to gauge-based rainfall products and near-surface meteorological observations indicated that the LTA improved the model's performance for most variables. The simulated precipitation with LTA using WWLLN lightning flashes in the hemispheric applications was significantly improved over the simulations without LTA when compared to precipitation from satellite observations in the Equatorial regions. The simulations without LTA showed significant sensitivity to the cumulus parameters (i.e., user-toggled switches) for monthly precipitation that was as large as 40% during convective seasons for monthly mean daily precipitations. With LTA, the differences in simulated precipitation due to the different cumulus parameters were minimized. The horizontal grid spacing of the modeling domain strongly influenced the LTA technique and the predicted total precipitation, especially in the coarser scales used for the hemispheric simulation. The user-definable cumulus parameters and domain resolution manifested the complexity of convective process modeling both with and without LTA. These results revealed sensitivities to domain resolution, geographic heterogeneity, and the source and quality of the lightning dataset.

1. Introduction

Thunderstorms are natural phenomena that have intrigued human imagination for thousands of years. Although early efforts in atmospheric science and modeling were focused on

understanding and forecasting thunderstorms, they remain difficult to accurately simulate in meteorological models. A variety of lightning parameterization schemes have developed in regional and global atmospheric models (Price and Rind, 1992; Romps et al., 2014; Finney, 2014; Lopez, 2016) based on various physical, dynamical, and cloud properties, but these schemes marginally reproduce the spatial and temporal variability of lightning flashes with varying success over different regions of the globe. With the advancement of lightning detection technologies both at ground level and via satellite in the past decades, observed lightning flashes with coverage from regional to global scales are available and can be used for lightning assimilation (LTA). A robust LTA can improve convective simulations in meteorological models for retrospective atmospheric simulations (e.g., Heath et al., 2016; Marchand and Fuelberg, 2015) or help generate better initial fields for real-time weather forecasting (e.g., Lagouvardos et al., 2013; Giannaros et al., 2016; Fierro et al., 2012, 2015) by pinpointing where deep convection occurred and altering the meteorology in what is generally referred to as a hot start (Gan et al., 2021). In addition, lightning also profoundly impacts the chemical composition of the troposphere by generating and releasing nitrogen oxides (LNO_x) that can significantly alter ground-level ozone (O_3) concentrations in some regions (Kang et al., 2020). Because meteorological models drive air quality simulations, improving meteorological variables with LTA will cascade to chemistry fields simulated by air quality models (Allen et al., 2012; Kang et al., 2019a,b). It is especially critical when LNO_x emissions are included in air quality models, since LTA is designed to align LNO_x emissions with the time and location when atmospheric convection occurred in the model, so the subsequent chemistry reactions and transport will more accurately reflect the emissions from lightning (Kang et al., 2019a and 2019b).

Heath et al. (2016) implemented an LTA technique in the Kain-Fritsch (KF) convective scheme (Kain, 2004) in the Weather Research and Forecasting (WRF) model, which extended the works of Rogers et al. (2000), Mansell et al. (2007), Lagouvardos et al. (2013), and Giannaros et al. (2016). In general, the lightning assimilation approach is straightforward, activating deep convection where lightning is observed and only allowing shallow convection where it is not. It was tested using WRFv3.8 simulations for several months in 2011 using lightning observations from the National Lightning Detection Network (NLDN) over the contiguous United States (CONUS). It was found that the simulation of warm-season rainfall was substantially improved, and other near-surface meteorological variables were clearly improved in retrospective WRF applications. The LTA technique has been implemented in subsequent WRF releases (not publicly available yet) and applied in many meteorology and air quality studies over the CONUS (e.g., U.S. EPA, 2019; Appel et al, 2021). Although using LTA improved the predicted meteorological variables, some occasional unwanted departures from base model predictions without LTA occurred. Most commonly, LTA resulted in a low bias in summertime rainfall in some regions (U.S. EPA, 2019).

For this reason, it is of interest to investigate two parameters associated with the KF convective scheme with different optional values, which are specified in the WRF runtime namelist input file, are often encountered by WRF users (https://www2.mmm.ucar.edu/wrf/users/docs/user_guide_v4/contents.html) . One parameter is called kfeta_trigger (also referred to as trigger for simplicity in this paper) which controls the conditions to determine how the KF convective scheme is triggered with three optional values: 1, the default value; 2, moisture-advection based trigger (only for ARW - the advanced research WRF dynamical solver); and 3, RH-dependent additional perturbation to Option 1 (not tested).

87 Another parameter is called cudt (namely **cu**mulus time interval, **d**elta **t**) and its value determines
88 the minutes between cumulus physics calls (here it is the KF scheme). The default value of 0
89 indicates that the cumulus physics is called at every model step, and any non-zero value specifies
90 the interval (minutes) that the cumulus physics is called (for example, cudt=10 means that the
91 cumulus physics is called every 10 minutes). Even though there are some discussions and
92 recommendations regarding the choice of these parameter values through online forums or WRF
93 user mailing list (e.g., https://forum.mmm.ucar.edu/; https://wrfems.info/;
94 https://www.epa.gov/sites/default/files/2017-02/documents/wrf_with_ltga_userguide.pdf), but
95 there is no literature evaluating how these parameter values impact model performance when
96 LTA is used.

97 The applications and evaluations of the LTA technique were limited to the CONUS,
98 reflecting the areal coverage of NLDN (Murphy et al., 2021). As the spatial applications of
99 atmospheric composition modeling are expanded from regional to hemispheric and global scales
100 and new lightning datasets are available, there is a strong need to examine how this LTA
101 technique performs at these larger scales when lightning flash data from a less accurate detection
102 network are used. Thus, lightning flashes from the World Wide Lightning Location Network
103 (WWLLN, operated by the University of Washington: http://www.wwlln.com) is a suitable
104 candidate because it has the global coverage, albeit its detection efficiency is lower than the
105 >95% of NLDN for cloud-to-ground (CG) flashes (Abarca et al., 2010).

106 Our research has multiple objectives based on the aforementioned open research needs:
107 1) assess the impact of the parameter values associated with the KF convective scheme on WRF
108 performance over the CONUS domain without LTA (BASE case) and with LTA using lightning
109 flashes from NLDN; 2) examine the LTA in WRF using lightning flashes from WWLLN and

compare to the simulations with NLDN lightning flashes; and 3) apply LTA to WRF simulations over the Northern Hemisphere and evaluate the performance in terms of precipitation and near-surface meteorological variables. In section 2, we describe the updates made to the initial LTA technique (Heath et al., 2016). Section 3 provides the detailed data and methodologies of the model simulations and their evaluation. Section 4 presents our analysis on the impact of parameters with KF convective schemes with and without lightning assimilation over CONUS using lightning flashes from NLDN and WWLLN. In section 5, we analyze the use of lightning flashes from WWLLN for LTA and evaluate WRF simulations with and without LTA over the Northern Hemisphere. And we conclude with key findings and recommendations in section 6.

2. Updates on the LTA technique

The lightning assimilation used here is based on Heath et al. (2016), and a full description of the method can be found in Heath et al. Here, we provide only the essential details, along with recent modifications to the scheme.

First, the lightning data (WWLLN or NLDN) is binned to the WRF domain in both time and space. The temporal binning is done every 30 min and includes lightning data from -10 min to +20 min of the current time. The spatial regridding searches for a lightning strike within each grid box (using the staggered grid edge coordinates) within each time bin. This process creates a new lightning file with the same horizontal dimensions as the WRF domain filled with zeros (no lightning) or ones (lightning) at each 30-minute time step. During the WRF simulation, if lightning is present, the scheme first goes through its standard updraft calculations, except that it uses the layer with the greatest moist static energy as its updraft source layer (USL). If the resulting cloud does not meet the criteria for deep convection, 0.1 g kg^{-1} of water vapor and 0.1 K are incrementally added to the USL until deep convection is forced. In the original Heath et

al. scheme, only moisture was added to the USL. We have included temperature perturbations to further promote activating deep convection in these grid points with lightning.

In the unmodified KF scheme, a cloud must exceed a minimum depth (as a function of cloud base temperature) to satisfy the deep convection criteria. Specifically, a cloud base temperature greater than 20ºC must have a cloud greater than 4 km deep. For a cloud base temperature less than 0ºC, the cloud depth only needs to be 2 km. For cloud bases between 0 – 20ºC, the minimum cloud depth is defined as $2000 + 100T_{LCL}$, where T_{LCL} is the temperature at the lifted condensation level (LCL) (Kain 2004). Heath et al. (2016) modified this depth for lightning assimilation to be more consistent with lightning-producing storms. Specifically, within WRF, storms with a base temperature greater than or equal to 20ºC must have a cloud depth of at least 6 km with a cloud top temperature less than -20ºC. Similarly, in the original model in Heath et al., storms with a cloud base temperature less than 20ºC must have a cloud depth of at least 4 km and a cloud top temperature less than -20ºC. These criteria were set to ensure that sub-grid deep convective clouds were deep enough to have a mixed-phase layer to support lightning (e.g., Mansell et al., 2007; Bruning et al., 2014; Preston and Fuelberg, 2015). In this study, we slightly modified the scheme to require that the cloud top is at least one model level above the -20ºC level, ensuring cloud-top temperatures are less than -20ºC (e.g., Stolzenburg and Marshall, 2009). The prior limit at -20ºC could inadvertently weaken simulated deep convective clouds, which may contribute to the dry bias in earlier applications of lightning assimilation approaches (U.S. EPA, 2019).

In Heath et al. (2016), if deep convection could not be achieved after incrementally adding up to 1 g kg^{-1} to the USL (which is now 1 g kg^{-1} and 1 K in our update), then no further action was taken, and deep convection was not activated by KF. However, to increase the

realism of the scheme and increase the odds of deep convection the next time the scheme is called, we have updated the approach as follows. If a deep convective cloud cannot be activated, the tallest cloud created is passed into the KF shallow convection scheme. In the KF scheme, shallow clouds are re-diagnosed each time the scheme is called. For example, suppose a shallow cloud is generated at t=0 and KF is called at 5 min intervals. In that case, at the t=5 min call, KF would determine if a shallow cloud is still present. Thus, the cloud can evolve so that at t=5 min it could have slightly different characteristics than the one diagnosed at t=0. This allows shallow clouds to grow, decay, or persist at short timescales.

Therefore, if the LTA method cannot trigger deep convection, the shallow cloud that is generated within WRF can precondition the atmosphere, thus increasing the likelihood of deep convection the next time the KF scheme with LTA is called. Therefore, these refinements to the LTA scheme in KF more closely replicate how convective initiation is observed in nature, where shallow cumulus and congestus clouds precondition the environment prior to deep convection initiation.

Lastly, at grid points without observed lightning, deep convection is suppressed in WRF, and only the shallow portion of KF is allowed to run (this is referred to as the "ShallowOnly" method). Because convective clouds in nature can form and precipitate without generating lightning, this suppression technique serves as a realistic approach to reproduce nature given the constraints of the KF parameterization.

3. Data and Methodology

3.1. Lightning flash data

178 Lightning flash data from two ground-based lightning detection networks were used for the
179 assimilation using the LTA technique in this study. The NLDN provides cloud-to-ground
180 lightning observations with a detection efficiency of >95% and a location accuracy of about 150
181 m (Murphy et al., 2021) over the contiguous U.S. (CONUS). The WWLLN provides global
182 lightning data with lower detection efficiency and location accuracy (Abarca et al., 2010;
183 Rudlosky and Shea, 2013; Burgesser, 2017) compared to NLDN and the Lightning Imaging
184 Sensor (LIS) observations (Mach et al., 2007). Since WWLLN has global coverage, even with its
185 relatively lower detection efficiency and location accuracy compared to NLDN, it could be a
186 good option for applications beyond CONUS. Figure 1 shows how the average lightning flash
187 rate (flashes $km^{-2}hr^{-1}$) from WWLLN compares to NLDN during July and September 2016 when
188 hourly lightning flash counts are gridded into the CONUS 12-km grid cells.

189 As shown in Figure 1, the lightning flash rates in NLDN are much higher than those in
190 WWLLN, especially during July and over the land, and this is generally true (not shown) that
191 NLDN reported more lightning flashes than WWLLN during warm months over land. The
192 differences are much smaller during cool months and over the coastal regions where NLDN has
193 coverage. Note that the absolute difference in flash count may not necessarily translate
194 proportionally into convective activities in terms of LTA because the LTA technique as
195 described in Heath et al. (2016) depends on the detection of lightning occurrence (binary "yes"
196 or "no" situation), not the actual flash count, in a specific time interval at a grid cell.

197 3.2. Precipitation Data

198 The daily precipitation from the Parameter-elevation Regressions on Independent Slopes
199 Model (PRISM)'s high-resolution spatial climate data for the United States
200 (https://climatedataguide.ucar.edu/climate-data/prism-high-resolution-spatial-climate-data-

201 united-states-maxmin-temp-dewpoint) is used to evaluate WRF-simulated precipitation over the
202 CONUS, and the NOAA Climate Prediction Center (CPC)'s global unified gauge-based analysis
203 of daily precipitation (https://psl.noaa.gov/data/gridded/data.cpc.globalprecip.html) product is
204 employed to assess WRF's hemispheric precipitation predictions. The daily total PRISM
205 precipitation data are available at 4-km horizontal grid spacing over the CONUS, and the annual
206 CPC precipitation (partitioned into daily totals) is available globally at 0.5° latitude × 0.5°
207 longitude grid (720 × 360) resolution. These datasets were regridded to the WRF modeling
208 domains for the 12-km CONUS and the 108-km Northern Hemisphere to pair with model
209 simulations in time and space. To assess the simulated precipitation over the oceans, especially
210 in the tropical regions where no gauge-based measurement is available, products from the Global
211 Precipitation Measurement (GPM) (Huffman et al., 2015; Asong et al., 2017), a joint mission co-
212 led by NASA and the Japan Aerospace Exploration Agency (JAXA) and comprised of an
213 international network of satellites that provide the next-generation global observations of rain
214 and snow, are employed. The Integrated Multi-satellitE Retrievals for GPM (IMERG) Long-term
215 Precipitation Data Products
216 (https://arthurhouhttps.pps.eosdis.nasa.gov/gpmdata/YYYY/MM/DD/imerg/; registration is
217 required for access) cover the entire globe with 0.1° latitude × 0.1° longitude grid resolution. To
218 compare with WRF simulated hemispheric precipitation, the daily mean precipitation data from
219 the IMERG V06 dataset (https://gpm.nasa.gov/data/directory) from 2016 is regridded onto the
220 hemispheric WRF domain. The research-quality gridded IMERG V06 dataset Final Run product
221 estimates precipitation using quasi-Lagrangian time interpolation, gauge data, and climatological
222 adjustment.
223 3.3. Ground-Based Meteorological Data

The impacts of user-definable parameter values associated with KF and datasets for LTA were quantified for simulated near-surface meteorological variables such as precipitation, 2-m temperature (T2), water vapor mixing ratio, wind speed and wind direction. The simulated meteorological fields from WRF are compared against observations from NOAA National Centers for Environmental Information (NCEI) land-based stations, which are archived from data collected globally (https://www.ncei.noaa.gov/products/land-based-station). The Atmospheric Model Evaluation Tool (AMET) (Appel et al., 2011) is used to pair surface observations with model predicted values in both space (bilinear interpolation) and time (hourly).

3.4. Model Configurations and Simulation Details

The WRF model (Skamarock and Klemp, 2008) version 4.1.1 (WRFv411, https://github.com/wrf-model/WRF/releases/tag/v4.1) with LTA updates to Heath et al. (2016) (as described in Section 2) is used to perform simulations over the CONUS and the hemispheric domains. The CONUS domain is configured with 36 vertical levels and 12-km horizontal grid spacing with 472 × 312 grid points. The hemispheric domain is configured with 45 vertical levels and 108-km horizontal grid spacing with 200 × 200 grid points that covers the entire Northern Hemisphere and the northern border of the Southern Hemisphere along the Equator. The simulation period for CONUS simulations is from April–July in 2016 with 10-day spin-up period from March 22; for the hemispheric domain, annual simulations for 2016 are performed. Our analysis focuses on July when convective activities are often the most prevalent over the CONUS; other months are examined in the hemispheric simulations which simulate the year-round convective activities in the tropics. The detailed configurations of cloud microphysics, land surface parameters, radiation schemes, and four-dimensional data assimilation (FDDA) are the same as described in Heath et al. (2016) and sample WRF namelist input files for both the

CONUS and hemispheric simulations are included in the supplementary information (Table S1 and Table S2). Data assimilation in the form of FDDA more specifically follows Heath et al. (2016) with updates noted in Gilliam et al. (2021) for the hemispheric domain where ~28 km NCEP Global Forecast System (GFS) analyses were used to nudge tropospheric temperature, moisture, and wind above the planetary boundary layer. For the CONUS domain the same nudging was applied, but 12 km North American Mesoscale (NAM) model analyses were leveraged. These two analysis datasets are a blend of short-term forecast with a comprehensive set of surface, upper-air, radar, aircraft, satellite, and other observations like sea-surface temperature that represent the best guess of the state of the atmosphere at any given time.

The KF scheme includes two options to trigger convective activity. Trigger 1 is based on a mass-conservative cloud model, which includes parameterized moist downdrafts, entrainment, and detrainment at the cloud edge (Kain and Fritsch, 1990, 1993) and allows interaction between cloud and environment, and it is the default option for most applications. Trigger 2 is an alternate option based on Ma and Tan (2009), and that is a moisture-advection modulated trigger function to improve results in subtropical regions when large-scale forcing is weak. In addition, the KF scheme is called by default at every time step, but it can be configured to only update convective parameters on a user-definable time increment. In this study, sensitivities are conducted to the version of the KF trigger (i.e., Trig1 and Trig2, abbreviated as K1 and K2 in Table 1, respectively), as well as to frequency at which KF is called (i.e., "cudt"). Two sensitivities on cudt were performed: one where KF is called at each model integration time step (i.e., "Cudt0", abbreviated as C0 in Table 1), and the other where KF is updated every 10 minutes of integration time (i.e., "Cudt10", abbreviated as C10 in Table 1). The time step is 1 minute (Table S1) and 3 minutes (Table S2) for the CONUS and hemispheric WRF simulations, respectively. The

sensitivities to KF trigger and update frequency are combined in a matrix of simulations that also are conducted with/without LTA, and they are listed in Table 1. All eight simulations are performed for both the CONUS and the hemispheric domains. For LTA cases, lightning flashes from both NLDN and WWLLN are used over the CONUS domain and lightning flashes from WWLLN are used for the hemispheric domain. For convenience of description, the cases without LTA are collectively referred to as BASE cases, and the cases with LTA are referred to as LTA cases. To further distinguish the lightning networks, the LTA cases are also referred to as LTA NLDN (or simply NLDN) and LTA WWLLN (or simply WWLLN) cases, respectively.

3.5. Evaluation Methodologies

The assessment of the impact of LTA on model performance is focused on precipitation since that is the most affected variable, though other near-surface variables are also evaluated. Due to the highly heterogeneous nature of thunderstorms and lightning over space, in addition to examining the overall statistics across the modeling domain, statistics are analyzed to assess the impact of LTA over U.S. climate regions (https://www.ncei.noaa.gov/monitoring-references/maps/us-climate-regions) in both domains and some of the larger countries in the hemispheric simulations. Figure 2 shows these climate regions over the CONUS modeling domain and the selected countries (also referred to as regions) in the hemispheric modeling domain.

The statistical metrics in this analysis include the widely used correlation coefficient (r) to measure the linear association of measured and simulated variables, mean bias (MB) and normalized mean bias (NMB) to quantify the departure of simulated values from measured values, and root mean square error (RMSE) and normalized mean error (NME) to elucidate the errors associated with model simulations. More emphasis is placed on certain metrics than others

depending on the nature of the simulated quantity. For instance, with precipitation, correlation coefficient (if the model can simulate rainfall at the right time and location) and MB and NMB (if the model over- or under-estimate rainfall amount) are more straightforward than the error metrics (though they are still relevant), but MB and NMB are inappropriate to evaluate wind directions.

4. CONUS WRF Simulations

As shown in Table 1, four BASE (without LTA) cases, four LTA cases using lightning flash data from NLDN, and four LTA cases using lightning flash data from WWLLN over the CONUS domain were performed using the combinations of two trigger options and two convective update (cudt) intervals, respectively. For the LTA cases, when lightning flashes were not present, the ShallowOnly option (Heath et al., 2016) was used (Table S1).

4.1. Precipitation

Figure 3 displays the July 2016 mean statistics generated by pairing the gridded WRF precipitation with the values from PRISM in time and space for each of the U.S. climatological regions. As shown in Figure 3, the BASE simulations present the more dramatic fluctuations among cumulus parameter sensitivities than the LTA cases. With Trig1, when the cudt is changed from 0 to 10, the correlation coefficient is substantially reduced across all the regions (Figure 3a), and increases in biases (overestimate of precipitation, Figures 3b&c) and errors (Figures 3d&e) are also worsened by less frequent cumulus updates. With trigger 2, the biases (MB and NMB) changed from overestimation to underestimation, and the errors (RMSE and NME) were smaller compared to Trig1. Though the setting for cudt altered simulations with Trig2, the difference was smaller than the cases with Trig1. In general, the Trig1 cases tended to

produce more precipitation (overestimate compared to PRISM precipitation) than the Trig2 cases (underestimate compared to PRISM precipitation), and the Cudt10 cases generated more precipitation than the Cudt0 cases. Among the four cases in the BASE model simulations, the K1C0 case (Trig1, Cudt0) is the most favorable in terms of the correlation coefficients and precipitation biases, but the error statistics, especially NME, may not be the most desirable.

Using LTA (Figure 3), the correlation coefficients significantly increased over the domain and across the regions (from the range of ~0.25 to ~0.40 to the range of ~0.30 to ~0.48) relative to the BASE cases. Though the LTA WWLLN cases had lower correlation compared to the LTA NLDN cases due to the lower detection efficiency of lightning flashes in WWLLN, the improvement was still rather considerable compared to the BASE cases. The biases in the LTA NLDN cases are most favorable with values negative but closest to zero (small underestimate). The LTA WWLLN cases produced larger negative biases than the BASE cases and LTA NLDN cases, again, related to detection efficiency of the networks. All the LTA cases (both NLDN and WWLLN) produced smaller errors than the BASE cases, and the differences between the NLDN cases and WWLLN cases were minimal. Comparing the LTA cases with the BASE cases, one noticeable feature is that with the different trigger and cudt values, all the statistics fluctuated dramatically from one case to another in the BASE cases, but fluctuation among the LTA cases was minimized and negligible. This is expected, as the moisture and temperature perturbations used to trigger convection with LTA (Section 2) will take precedence over the trigger options and grouping the lightning data into 30-minute bins should mitigate the influence of the cudt option. These features were deliberately incorporated into the LTA technique for precisely these reasons, but this paper documents their systematic testing.

Examination of the statistics across the climatological regions over the CONUS domain indicates that the Ohio Valley (OVC) stands out among all the regions with the lowest correlation coefficients and largest RMSE values in all the BASE cases. However, with LTA, the correlation coefficients in OVC were brought to the median range among other regions, though the RMSE values were still the largest in that region; these features in OVC are more understandable as manifested in Figure 12, examined in detail in Section 5. Other statistics in OVC with LTA were comparable with other regions except for relatively larger negative MB values associated with the LTA WWLLN cases. Another obvious characteristic with regards to correlation coefficients and errors (RMSE and NME) was that there was more spread among the regions in the LTA cases than in the BASE cases (except in OVC), which resulted from the geographically heterogeneous nature of convective precipitation and the associated observed lightning intensity across the regions.

To alleviate the underestimation of precipitation in the LTA WWLLN cases, additional simulations (K1C10Ws0 and K2C10Ws0; where K1C10W and K2C10W are the same as in Table 1, while s0 means zero suppress when lightning flash is not present) were performed by switching the suppression option as described in Heath et al. (2016) from "ShallowOnly" to "NoSuppress." This modification still triggers deep convection where lightning is observed; however, at grid points without lightning, the KF scheme is configured to run normally (i.e., the same as in the BASE cases). As shown in Figure S1, the correlation coefficients in the WWLLN+s0 cases were comparable with other LTA cases, and the values in the K2C10Ws0 case were similar to the NLDN cases and improved upon the K1C10W case. The MB in the WWLLN+s0 cases were mostly positive (overestimate), which is expected because the KF scheme has more freedom to activate deep convection. The K2C10Ws0 case produced the most

361 desirable results (domain mean MB is nearly zero) among all the cases. However, the biases
362 associated with LTA simulations using the "NoSuppress" option are affected by both the
363 lightning detection efficiency and the domain resolutions, which is more evident in the LTA
364 simulations over the hemispheric domain in Section 5.

365 4.2. Other Near-Surface Meteorological Variables

366 Besides precipitation, T2, water vapor mixing ratio, wind speed, and wind direction are
367 also analyzed. As shown in Figure 4, T2 in the BASE cases has correlation coefficients over the
368 CONUS domain and all the regions ranging from ~0.95–0.98. With LTA, the correlations for T2
369 were further improved for all the regions, with WWLLN cases performing slightly worse than
370 the NLDN cases. The impact of cumulus parameters on correlations was minimal for the BASE
371 and LTA cases. However, the cumulus parameters seem to impact the biases (MB and NMB,
372 Figures 4b,c) and errors (RMSE and NME, Figure 4d,e) in the BASE cases across all the regions,
373 and like precipitation, all the LTA cases minimized the impact of different cumulus parameter
374 values. All the LTA cases reduced the errors (RMSE and NME) associated with T2 across all the
375 regions, with NLDN slightly better than WWLLN. In summary, the T2 statistics were improved
376 by using LTA, and the WWLLN cases were comparable to the NLDN cases with a slight
377 degradation for all the regions.

378 The 2-m water vapor mixing ratios metrics (Figure 5) of the cases, in general, resemble
379 those of T2, in that the LTA cases have slightly increased the correlation coefficients from the
380 already well-simulated BASE cases. More spread occurs for biases (MB and NMB, Figures 5b,c)
381 and within the BASE cases for errors (RMSE and NME, Figures 5d,e). Regional spread in these
382 statistics is attributed to the diverse air mass types that drive large differences in the moisture

content and convective activity. Even though the values were low for both errors and biases (< 0.5%), using either LTA technique is an improvement over the BASE cases.

The cumulus parameters and LTA showed less impact on the correlations for 10-m wind speed, but the impacts on biases and errors were noticeable (Figure 6). All the model cases underestimate wind speed (~5–12%, depending on regions and model cases), and the cumulus parameters caused relatively large differences in the metrics of the BASE cases with both trigger and cudt options contributing most. Overall, using Trig2 with Cudt10 is most favorable in terms of biases (less underestimate) and errors (smaller errors) among the BASE cases. In all the LTA cases, the underestimation was reduced when compared to the BASE cases, and errors were reduced with negligible differences among the cases with different cumulus parameters and assimilating lightning data from the different networks. Similar behavior was observed for wind direction where only correlation coefficient, MB, and RMSE are displayed in Figure S2 because normalized metrics do not apply.

5. Northern Hemispheric WRF Simulations

As shown in Table 1, the model cases performed over the Northern Hemisphere are similar to those performed over the CONUS, but with LTA cases using lightning data from WWLLN that was gridded on the domain with 108-km horizontal grid spacing.

5.1. Precipitation

Before comparing the simulated precipitation with available observations, the examination begins with how the WRF-simulated precipitation with and without LTA compares spatially over the Northern Hemisphere. Figure 7 displays the mean daily precipitation during July 2016 from

two LTA cases and two BASE cases (Trig1 and Trig2) and the corresponding differences between LTA and BASE (LTA – BASE) cases with the same trigger values, and Figure S3 presents the mean daily precipitation differences between HK1C0W and HK1C0B cases throughout 2016. Compared to the BASE cases, the LTA cases produced significantly less rainfall along the Equatorial regions but generally more rainfall away from the Equator, especially over the midlatitude land regions. Because no gauge-based observational data are available over the ocean, the IMERG precipitation for July 2016 is presented in Figure 7g with the difference plots from the base case (HK1C0B) and the LTA case (HK1C0W) being displayed in Figures 7h and 7i, respectively. Over the Equatorial regions, the precipitation simulated by the LTA cases (Figures 7b and 7e) more closely resembled the IMERG precipitation than the BASE cases. The difference plots clearly indicate that the base cases significantly overestimated, and the LTA cases slightly underestimated the precipitation over large areas in the Equatorial regions. Similar results persisted throughout the year as shown in Figure S4 (the difference of mean daily precipitation by month between the base case, HK1C0B, and the IMERG product) and Figure S5 (the difference of mean daily precipitation by month between the LTA case, HK1COW, and the IMERG product). Next, the WRF simulated precipitation is compared with the CPC gauge-based analysis values over land. Figure 8 displays the CPC rainfall and simulated mean daily precipitation during July 2016 along with the estimates from the LTA and BASE cases with different cumulus parameters. Since the gauge-based observational values are only available over land, the simulated values in Figure 8 are only displayed over land. As shown in Figure 8, all the model cases simulated the overall spatial pattern of higher values in the tropical regions and lower values in high latitude regions. However, subtle differences existed from case to case in different regions. For example, the HK1C10B case (Figure 8d) and the HK2C10B case (Figure 8f) produced the highest and the lowest

428 precipitation over Africa and South America (along the Mexico coast to the South American
429 continent) within the modeling domain.

430 All the LTA cases uniformly produced larger correlation coefficients than the BASE
431 cases (Figure 9) when and where convective activities were prevalent. In the U.S., convective
432 activities occur during warm months (from May to September), while in Mexico and India,
433 convection is active throughout the year. In Canada, convective activities are less frequent
434 because of the cooler temperatures and low moisture at the high latitude. When and where
435 convection was active, the cumulus parameters produced significant differences in modeled
436 convective activity, as correlation coefficients are higher in the BASE cases with Trig1. Same as
437 the simulations over the CONUS domain, the cumulus parameters had a minor impact on the
438 correlation coefficients for the LTA cases regardless the regions. This indicates that, even with
439 the less dense WWLLN lightning observations, using LTA improves the timing and location of
440 deep convection.

441 RMSE were comparable for all the model cases across the selected regions (Figure 10),
442 with the LTA cases pointing to lower values than the BASE cases at all the regions except for the
443 U.S. where the LTA and BASE cases alternated to have slightly lower RMSE values over each
444 other during the year. Alternatively, the MB values varied significantly among the model cases
445 and across the regions as shown in Figure 11. One common feature is that the differences among
446 the LTA cases were small, but two distinctly separate groups among the BASE cases were noted
447 in all the regions; the cases with Trig1 had always significantly greater precipitation values than
448 the cases with Trig2. In China and Mexico, all the simulations overestimated the precipitation
449 through the year except for small underestimate during the cool months (October–December). In
450 India, the overestimate and underestimate were equally split among the model cases, with

dramatic changes from month to month in the same model case. The behavior of MB values among the model cases and through the year was more stable for the U.S. (to a lesser extent in Canada) than in other regions, in which the BASE cases with Trig1 have the best performance (MB values near zero), the BASE cases with Trig2 significantly underestimated precipitation over land during convective season, and all the LTA cases overestimated precipitation over land during the warm months. Here we offer two plausible explanations for the drastically different behaviors of the MB values associated with precipitation in different regions.

First, from the modeling point of view, the WRF model is widely studied and applied in North America, especially in the U.S. As a result, more accurate observation-based datasets are available to nudge WRF through FDDA (Liu et al., 2008), and all the work has led to the best performance over the U.S. for the recommended default set of convective trigger and update frequency for the cumulus scheme. Second, from the observational point of view, the CPC rainfall dataset is built upon field gauge measurements that may vary in accuracy and consistency from county to county. As shown in Figure S6, the NMB values were generally in the range of -50% to 50% in the U.S. and Canada (comparable to the NMB values for the 12-km CONUS simulations against PRISM precipitation as shown in Figure 3c), but in other countries, especially during cool months, the values were up to hundreds or even thousands of percent that suggests possible few observations available in the denominator in NMB calculations. For instance, the highest NMB value in China coincided with the Spring Festival that is often a long holiday for China suggesting possible gaps for data collection.

We next focus on the high MB values associated with the LTA cases in the U.S. Consistent in the analysis in Figure 3b, the LTA WWLLN cases over the 12-km CONUS domain always had larger negative MB (underestimates) than the LTA NLDN cases due to the lower

detection efficiency of lightning flashes in WWLLN than in NLDN. However, in the 108-km hemispheric simulations, the same WWLLN datasets produced large positive MB (overestimates) for precipitation. To understand this phenomenon, we need to first examine how the LTA method works. Because it uses a yes/no lightning indicator to trigger convection, 108-km grid spacing might be too coarse for such a simplistic approach to work. For example, one lightning strike within a 108-km grid cell will trigger deep convection, which, because of the large spatial coverage of the grid cell, can contribute to the high bias in precipitation because convective rainfall is realistically more localized. Although the KF scheme sets a fixed radius for thunderstorms (e.g., Equation 6 in Kain 2004), applying the resulting rain over the entire 108-km × 108-km grid box could partially explain the excess rainfall. This may also be explained by the fact that the convective time-scale formulation in KF scheme was originally developed at grid lengths of 20–25 km (Sims et al., 2017). A potential developmental pathway for the LTA method at these scales is to test different thresholds of the 30-min flash density to ensure sufficient lightning is present to trigger deep convection. Overall, compared to the CPC rainfall, the LTA technique significantly improved the temporal and spatial correlation of convective precipitation, but the precipitation amount was overestimated over the U.S. and other regions for the 108-km modeling domain.

To further examine the impact of modeling domain resolutions on convective precipitation, Figure 12 displays the spatial precipitation from PRISM, CPC (regridded onto the 12-km CONUS domain), and simulated precipitation from one BASE case and two LTA cases with NLDN and WWLLN data, respectively, over the 12-km CONUS domain and one LTA case over the 108-km hemispheric domain that has been regridded to the 12-km CONUS domain. As shown in Figures 12a,b, the two observation-based precipitation products, PRISM and CPC,

497 compared well to each other, noting that the PRISM product displays more subtle granularity
498 than the CPC product due to the large difference in spatial resolutions (4-km for PRISM versus
499 0.5° for CPC). The overall spatial pattern of mean daily precipitation was captured by both the
500 12-km LTA simulations (Figures 12d,e), and the 108-km LTA simulation (Figure 12f). The
501 heaviest rainfall was centered in the OVC area in the observation-based and the simulated
502 precipitation maps, but the shape and spread of the rain band were different. The rain band in the
503 12-km BASE case (Figure 12c) was more spread and scattered with southwest-to-northeast
504 orientation, while the observation-based products and the LTA cases indicated a relatively
505 smaller area with west-east direction. Thus, the LTA cases (12-km CONUS simulations)
506 compared better to the observation-based products spatially than the BASE case. The K2C10W
507 case (with WWLLN) tended to produce less precipitation than the K2C10N case (with NLDN)
508 and both observation-based products. These spatial discrepancies for precipitation in OVC
509 between PRISM and the model cases were reflected by the unique statistical behavior as
510 displayed in Figure 3 and discussed in Section 4.1. As a likely artifact of excessively activated
511 convection within the 108-km grid cells with a spatial scale much larger than most thunderstorm
512 scales, the HK2C10W case indicated areas of heavy precipitation that were also shown in the
513 observation-based products and the 12-km LTA cases (both K2C10W and K2C10N) at
514 approximately same locations but with much less spatial extent. To resonate with the large
515 discrepancies in the MB values shown in Figure 11a among the BASE cases, the precipitation
516 from HK2C10B and HK2C10B cases is similarly displayed in Figures 12g,h. The case with
517 Trig1 was clearly more comparable to the CONUS cases than the Trig2 case in that the
518 precipitation from Trig2 was severely underestimated across the entire U.S. These hemispheric
519 simulations amplified the impact of the trigger options on precipitation during warm months

among the BASE cases, resulting in differences in daily total precipitation of up to 40% in the U.S. (Figure S6a). These results underscore the need to carefully set cumulus parameters for the KF scheme in WRF simulations.

The mismatch of the spatial scales between domain resolution and thunderstorms in the 108-km simulations is a limitation of current LTA scheme that could be improved in future development. In addition to using lightning density to trigger convection, another option is to implement the LTA scheme in the MultiScale Kain-Fritsch (MSKF) scheme (Glotfelty et al., 2019; Zheng et al., 2016), a "scale-aware" variant of KF that refines the convective tendencies based on the grid spacing used in the simulation.

5.2. Impact on Other Meteorological Variables

The impact of the cumulus parameters and LTA scheme on near-surface meteorological variables of the 108-km hemispheric simulations are evaluated like the 12-km CONUS simulations. However, due to the lack of observation data beyond North America, the analysis is mainly focused on the U.S. regions, but all the available data within the hemispheric domain is collectively referred to as "ALL" regardless of where the data originated. Affected by the coarser domain resolution, all the statistical measures for T2 (Figure 13) from the hemispheric simulations indicated degradations in model performance relative to the 12-km CONUS domain (Figure 4). As in the CONUS simulations, the LTA cases increased correlation coefficients and decreased errors (RMSE and NME) compared to the BASE cases. Like the CONUS simulations, the cumulus parameters minimally affected the LTA cases, while significant deviations were produced among the BASE cases. Unlike the CONUS simulations where both trigger and cudt contributed to T2 differences, the large differences among the BASE cases for the hemispheric simulations were attributed to the trigger options. Though all the cases tended to underestimate

T2 (contrary to the CONUS simulations where T2 was generally overestimated), among the BASE cases, greater underestimates were associated with Trig1 than Trig2. The LTA cases uniformly underestimated T2 consistent with the Trig1 BASE cases. The performance of hemispheric simulations for 2-m water vapor mixing ratio (Figure 14) resembles T2 in the comparison to the CONUS simulations (Figure 5), which produced smaller correlation coefficients and larger errors and biases (mainly overestimates for both CONUS and hemispheric simulations). Without exception, the LTA cases consistently performed better in terms of correlation coefficients and errors than the BASE cases. However, different from other meteorological variables, the MB and NMB associated with water vapor mixing ratio are affected by both cumulus parameters (trigger and cudt) for all the model cases (both BASE cases and LTA cases). The LTA cases with Trig1 performed better than the cases with Trig2, and with the same trigger value, cudt=0 is preferable to cudt=10; however, for the BASE cases, it was the opposite, though with smaller differences. At the 108-km grid spacing, the 10-m wind speed (Figure S7) and wind direction (not shown) statistics were comparable among the cumulus parameters and the application of LTA.

6. Discussion and Recommendations

This study corroborated that the simple observation-based LTA scheme implemented in Heath et al. (2016) improved WRF simulated precipitation and other near-surface meteorological variables as evidenced by the simulations over multiple spatial scales and over a longer test period. Testing on a 12-km CONUS domain using lightning flashes from WWLLN instead of NLDN slightly reduced the correlation coefficients and locally increased errors due to the lower detection efficiency of WWLLN. The update of the LTA technique reduced the underestimate of precipitation that was often reported in the application of WRF simulations conducted over the

CONUS domain (U.S. EPA, 2019). Changing lightning flash data from NDLN to WWLLN resulted in additional underestimate of precipitation due to fewer lightning flashes in WWLLN than the NLDN dataset. However, when the WWLLN data was used in the hemispheric simulations, the model performance for precipitation over the Equatorial regions was significantly improved from significant overestimation in the base cases to slight underestimation in the LTA cases, and the precipitation over land was generally overestimated during the convective season for almost all the selected regions, especially over North America.

The application of LTA in the hemispheric simulations with a 108-km domain exposed a shortcoming of this simple LTA scheme. When the model grid cell is substantially larger than most thunderstorm scales (Murphy and Konrad II, 2005), over-triggering of convection within the entire grid cell leads to overestimated precipitation. With the current LTA implementation and the high lightning detection efficiency network, such as NLDN, the 12-km grid spacing is suitable for LTA because thunderstorms often have a radial distance of 1–10 km. When lightning data from low detection efficiency networks (such as WWLLN) are used over finer resolution domains (≤12 km), the "NoSuppress" option with LTA could balance increasing precipitation while maintaining reasonable levels of uncertainty in the other variables for a more holistic model evaluation. The effect of domain resolution on precipitation simulation with LTA portends further development and improvement of the LTA technique. Two potential developmental directions are to use criteria values of lightning flash density dependent on grid resolution to trigger deep convection and/or to implement the LTA scheme in the MSKF scheme in WRF to adapt to different simulation scales. Preliminary experimentation on the 108-km scale (not shown) suggests that MSKF could improve these comparisons with observations (compared

589 to the KF scheme presented here), including better cloud and precipitation fields (Hogrefe et al.,
590 2021).

591 The experiment of cumulus parameters (trigger and cudt) associated with the KF scheme was
592 performed for both the CONUS and hemispheric WRF simulations. Results revealed several key
593 behaviors in both the BASE case simulations and LTA case simulations. First, the BASE case
594 simulations were sensitive to both trigger and cudt options over the CONUS domain, but only
595 trigger options produced significant variations for the hemispheric simulations. Second, the
596 impact of the cumulus parameters on LTA cases was insignificant for both modeling domains.
597 Separately, the original LTA technique as described in Heath et al. (2016) showed influence
598 from the cumulus parameters on the LTA cases (Figure S8), but after implementing the updated
599 cloud top height (one model level above -20° C) and the additional pre-conditioning shallow
600 convection (see Section 2), the fluctuations among the LTA cases were significantly reduced.
601 Third, the most pronounced impact of cumulus parameters was on the amount of precipitation in
602 the BASE cases. The Trig1 option generated up to a 10% overestimate of month-mean daily
603 precipitation over the CONUS with cudt=0 and an additional 10–15% overestimate with cudt=10
604 during July 2016. With Trig2, the simulated precipitation became underestimated by about 10–
605 15%, with the cudt contributing to ~5% difference; Cudt10 had less underestimate than Cudt0.
606 However, over the hemispheric domain, only the trigger option dramatically affected simulated
607 precipitation; during the summer months (June, July, and August), the Trig2 cases
608 underestimated the mean daily precipitation by up to 40% more than the Trig1 cases that
609 matched the observation-based precipitation products within 10%. In summary, without LTA,
610 the recommended default values (trigger=1 and cudt=0) by WRF documentation remain the best

611 option for both the CONUS and hemispheric simulations to achieve the best model performance,
612 especially for North America, and with LTA, all the options performed equally well.
613 As one of the most prominent meteorological models, WRF has been widely used in a variety
614 of applications from regional to global scales and from weather and climate studies to air
615 pollution transport in air quality forecast and regulatory compliances. It is important to improve
616 the convective processes (e.g., convective transport of air pollutants matching the times and
617 locations of lightning NO_x production) to have more accurate precipitation and other
618 meteorological fields with more resources being available including observational datasets,
619 computing capability, and advanced scheme development. Observation-based data assimilation
620 has been historically proven to be one of the most effective methods to improve model's
621 performance in time and space. This research is emerging to consider and use the lightning
622 observations that have become available in various formats and scales in the past decades to
623 improve convection simulations through LTA. Additional networks of lightning observations
624 and more detailed properties associated with the process of lightning discharge are becoming
625 available (such as the strokes per flash, the strength of lightning energy level, and the separation
626 of cloud-to-ground and inter- or intra-cloud strikes being more accurately quantified, especially
627 with the available satellite lightning products from Geostationary Lightning Mapper (GLM)
628 detection systems borne on the GOES-16 and -17 satellites (Goodman et al., 2013)).
629 Accordingly, lightning assimilation techniques will continue to evolve and build upon the
630 research presented here.
631

Code and data availability

The WRF model is available for download through the WRF website (http://www.wrf-model.org/index.php). The LTA code is not publicly available yet but interested users can contact the corresponding author to acquire the source code. The raw lightning flash observation data can be purchased through Vaisala Inc. (https://www.vaisala.com/en/products/systems/lightning-detection), and the WWLLN raw data are also available for purchase at http://wwlln.net. The immediate data except the lightning flash data behind the figures are available from doi: https://doi.org/10.5281/zenodo.6493145. PRISM Precipitation data for the United States are retrieved from https://climatedataguide.ucar.edu/climate-data/prism-high-resolution-spatial-climate-data-united-states-maxmin-temp-dewpoint and the CPC Global Unified Precipitation data provided by the NOAA/OAR/ESRL PSL, Boulder, Colorado, USA, from their Web site at https://psl.noaa.gov/data/gridded/data.cpc.globalprecip.html. The IMERG data were provided by the NASA/Goddard Space Flight Center's Precipitation Measurement Missions (PMM) Science Team and Precipitation Processing System (PPS), which develop and compute the IMERG as a contribution to GPM, and archived at the NASA GES DISC.

Author contributions. DK conceptualized the study, performed the model simulation and data curation, carried out the analysis, and wrote the paper. NH developed the mechanism and software and wrote the paper. RG prepared the scripts for model simulations and data analysis and edited the paper. TS supervised the research, provided resources, and edited the paper. JP edited the paper.

Competing interests. The authors declare that they have no conflict of interest.

Disclaimer: This paper has been subjected to an EPA review and approved for publication. The views expressed here are those of the authors and do not necessarily reflect the views or policies of the U.S. Environmental Protection Agency (EPA).

Acknowledgement:

We thank Jerry Herwehe and Kiran Alapaty at the EPA for reviewing the paper and providing valuable comments and suggestions. We give our sincere thanks to Dr. Lisa Neef and the other anonymous referee for their comments and many suggested changes that improved the clarity and readability of this paper.

References

Abarca, S. F., Corbosiero, K. L., and Galarneau Jr., T. J.: An evaluation of the Worldwide Lightning Location Network (WWLLN) using the National Lightning Detection Network (NLDN) as ground truth, J. Geophys. Res., 115, D18206, doi:10.1029/2009JD013411, 2010.

Allen, D. J., Pickering, K. E., Pinder, R. W., Henderson, B. H., Appel, K. W., and Prados, A.: Impact of lightning-NO on eastern United States photochemistry during the summer of 2006 as determined using the CMAQ model, Atmos. Chem. Phys., 12, 1737–1758, 2012.

Appel, K. W., Gilliam, R. C., Davis, N., Zubrow, A., and S. C. Howard, S. C.: Overview of the Atmospheric Model Evaluation Tool (AMET) v1.1 for evaluating meteorological and air quality models, Environ. Modell. Software, 26, 434–443, doi:10.1016/j.envsoft.2010.09.007, 2011.

Appel, K. W., Bash, J. O., Fahey, K. M., Foley, K. M., Gilliam, R. C., Hogrefe, C., Hutzell, W. T., Kang, D., Mathur, R., Murphy, B. N., Napelenok, S. L., Nolte, C. G., Pleim, J. E., Pouliot, G. A., Pye, H. O., Ran, L., Roselle, S. J., Sarwar, G., Schwede, D. B., Sidi, F. L., Spero, T. L., and Wong, D. C.: The Community Multiscale Air Quality (CMAQ) model versions 5.3 and 5.3.1: system updates and evaluation, Geosci. Model Dev., 14, 2867–2897, https://doi.org/10.5194/gmd-14-2867-2021, 2021.

Asong, Z. E., Razavi, S., Wheater, H. S., and Wong, J. S.: Evaluation of Integrated Multisatellite Retrievals for GPM (IMERG)over Southern Canada against Ground Precipitation Observations:A Preliminary Assessment, J. Hydrometeorology, 18, 1033-1050, https://doi.org/10.1175/JHM-D-16-0187.1, 2017.

Bruning, E. C., Weiss, S. A., and Calhoun, K. M.: Continuous variability in thunderstorm primary electrification and an evaluation of inverted-polarity terminology, Atmos. Res., 135–136, 274–284, doi:10.1016/j.atmosres.2012.10.009, 2014.

Burgesser, R. E.: Assessment of the World Wide Lightning Location Network (WWLLN) detection efficiency by comparison to the Lightning Imaging Sensor (LIS), Q. J. R. Meteorol. Soc. 143: 2809–2817, doi:10.1002/qj.3129, 2017.

690 Fierro, A. O., Mansell, E. R., Ziegler, C. L., and MacGorman, D. R.: Application of a lightning data
691 assimilation technique in the WRFARW model at cloud-resolving scales for the tornado outbreak of
692 24 May 2011, Mon. Weather Rev., 140, 2609–2627, 2012.
693 Fierro, A. O., Clark, A., Mansell, E. R., MacGorman, D. R., Dembek, S. R., and Ziegler, C. L.: Impact of
694 storm-scale lightning data assimilation on WRF-ARW precipitation forecasts during the 2013 warm
695 season over the contiguous United States, Mon. Weather Rev., 143, 757–777, 2015.
696 Finney, D. L., Doherty, R. M., Wild, O., Huntrieser, H., Pumphrey, H. C., and Blyth, A. M.: Using cloud
697 ice flux to parametrise large-scale lightning, Atmospheric Chemistry and Physics, 14 (23),
698 12,66512,682, doi:10.5194/acp-14-12665-2014, 2014.
699 Gan, R., Yang, Y., Xie, Q., Lin, E., Wang, Y., and Liu, P.: Assimilation of Radar and Cloud-to-Ground
700 Lightning Data Using WRF-3DVar Combined with the Physical Initialization Method—A Case
701 Study of a Mesoscale Convective System. J. Meteorol. Res. 35, 329–342.
702 https://doi.org/10.1007/s13351-021-0092-4, 2021.
703 Giannaros, T. M., Kotroni, V., and Lagouvardos, K.: WRF-LTNGDA: A lightning data assimilation
704 technique implemented in the WRF model for improving precipitation forecasts, Environ. Modell.
705 Software, 76, 54–68, 2016.
706 Gilliam, R. C., Herwehe, J. A., Bullock, Jr, O. R., Pleim, J. E., Ran, L., Campbell, P. C., & Foroutan, H.:
707 Establishing the suitability of the model for prediction across scales for global retrospective air
708 quality modeling. J. Geophys. Res.: Atmospheres, 126, e2020JD033588,
709 https://doi.org/10.1029/2020JD033588, 2021.
710 Glotfelty, T., Alapaty, K., He, J., Hawbecker, P., Song, X., and Zhang, G.: The Weather Research and
711 Forecasting Model with Aerosol–Cloud Interactions (WRF-ACI): Development, evaluation, and
712 initial application, Mon. Wea. Rev., 147, 1491–1511, doi:10.1175/MWR-D-18-0267.1, 2019.
713 Goodman, S. J., Blakeslee, R. J., Koshak, W. J., Mach, D., Baiely, J., Buechler, D., Carey, L., Schultz, C.,
714 Bateman, M., McCaul Jr., E., and Stano G.: The GOES-R Geostationary Lightning Mapper (GLM),
715 Atmos. Res., 125-126, 34-49, doi: 10.1016/j.atmosres.2013.01.006, 2013.

716 Heath, N. K., Pleim, J. E., Gilliam, R. C., and Kang, D.: A simple lightning assimilation technique for
717 improving retrospective WRF simulations, J. Adv. Model. Earth Syst., 8, 1806–1824,
718 https://doi.org/10.1002/2016MS000735, 2016.
719 Hogrefe, C., Gilliam, R., Mathur, R., Henderson, B., Sarwar, G., Appel, K. W., Pouliot, G., Willison, J.,
720 Miller, R., Vukovich, J., Eyth, A., Talgo, K., Allen, C., and Foley, K.: CMAQv5.3.2 ozone
721 simulations over the Northern Hemisphere: model performance and sensitivity to model
722 configuration. 20th Annual CMAS Conference, November 1–5, 2021, Virtual, 2021.
723 Huffman, G. J., Adler, R. F., and Nelkin, E. J.: Integrated Multi-satellitE Retrievalsfor GPM (IMERG)
724 technical documentation. NASA/GSFC Code612 Tech. Doc., 48 pp. [Available online at
725 http://pmm.nasa.gov/sites/default/files/document_files/IMERG_doc.pdf.], 2015.
726 Kain, J. S.: The Kain-Fritsch convective parameterization: An update, J. Appl. Meteorol., 43(1), 170–181,
727 doi:10.1175/1520-0450(2004)043<0170:TKCPAU>2.0.CO;2, 2004.
728 Kain, J.S. and Fritsch, J. M.: A one-dimensional entraining/detraining plume model and its application in
729 convective parameterization, J. Atmos. Sci., 47, pp. 2784-280,1990.
730 Kain, J.S. and Fritsch, J. M.: Convective parameterization for mesoscale models: the Kain–Fritsch
731 scheme, The Representation of Cumulus Convection in Numerical Models, Meteor. Monogr., No. 46,
732 Amer. Meteor. Soc., pp. 165-170, 1993.
733 Kang, D., Mathur, R., Pouliot, G. A., Gilliam, R. C., and Wong, D. C.: Significant ground-level ozone
734 attributed to lightning-induced nitrogen oxides during summertime over the Mountain West States,
735 npj Climate and Atmospheric Science 3, doi: 10.1038/s41612-020-0108-2, 2020.
736 Kang, D., Pickering, K., Allen, D., Foley, K., Wong, D., Mathur, R., and Roselle, S.: Simulating
737 Lightning NO Production in CMAQv5.2: Evolution of Scientific Updates, Geosci. Model Dev. 12,
738 3071-3083, https://doi.org/10.5194/gmd-12-3071-2019, 2019a.
739 Kang, D., Foley, K., Mathur, R., Roselle, S., Pickering, K., and Allen, D.: Simulating Lightning NO
740 Production in CMAQv5.2: Performance Evaluations, Geosci. Model Dev. 12, 4409–4424,
741 https://doi.org/10.5194/gmd-12-4409-2019, 2019b.

742 Lagouvardos, K., Kotroni, V., Defer, E., and Bousquet, O.: Study of a heavy precipitation event over
743 southern France, in the frame of HYMEX project: Observational analysis and model results using
744 assimilation of lightning, Atmos. Res., 134, 45–55,2013.
745 Liu, Y., Warner, T. T., Bowers, J. F., Carson, L. P., Chen, F., Clough, C. A., Davis, C.A., Egeland, C. H.,
746 Halvorson, S. F., Huck Jr., T. W., Lachapelle, L., Malone, R. E., Rife, D. L., Sheu, R. -S., Swerdlin,
747 S. P., and Weingarten, D. S.: The operational mesogamma-scale analysis and forecast system of the
748 U. S. Army Test and Evaluation Command. Part 1: Overview of the modeling system, the forecast
749 products, J. Appl. Meteorol. Climatol., 47, 1077–1092, 2008.
750 Lopez, P.: A lightning parameterization for the ECMWF Integrated Forecasting System, Monthly
751 Weather Review, 144 (9), 30573075, doi:10.1175/mwr-d-16-0026.1, 2016.
752 Ma, L.-M., and Tan, Z. M.: Improving the Behavior of the Cumulus Parameterization for Tropical
753 Cyclone Prediction: Convection Trigger. Atmospheric Research, 92, 190-211.
754 https://doi.org/10.1016/j.atmosres.2008.09.022, 2009.
755 Mach, D. M., Christian, H. J., Blakeslee, R. J., Boccipio, D. J., Goodman, S. J., and Boeck, W. L.:
756 Performance assessment of the Optical Transient Detector and Lightning Imaging Sensor, J. Geophys.
757 Res.,112, D09210, doi:10.1029/2006JD007787, 2007.
758 Mansell, E. R., Ziegler, C. L., and MacGorman, D. R.: A lightning data assimilation technique for
759 mesoscale forecast models, Mon. Weather Rev., 135, 1732–1748, doi:10.1175/MWR3387.1, 2007.
760 Marchand, M. R., and Fuelberg, H. E.: Assimilation of lightning data using a nudging method involving
761 low-level warming, Mon. Weather Rev., 142, 4850–4871, doi:10.1175/MWR-D-14-00076.1., 2015.
762 Murphy, M. J., Cramer, J. A., and Said, R. K.: Recent history of upgrades to the U.S. National Detection
763 Network, J. Atmos. Ocean. Tech., 38, 573-581, doi:10.1175/JTECH-D-19-0215.1, 2021.
764 Murphy, M. S., and Konrad II, C. E.: Spatial and temporal patterns of thunderstorm events that produce
765 cloud-to-ground lightning in the interior southeastern United States, Monthly Weather Review, 133,
766 1417-1420,2005.

767 Preston, A. D., and Fuelberg, H. E.: Improving lightning cessation guidance using polarimetric radar data,
768 Weather Forecasting, 30, 308–328, doi:10.1175/WAF-D-14-00031.1, 2013.
769 Price, C., and Rind D.: A simple lightning parameterization for calculating global lightning distributions,
770 Journal of Geophysical Research: Atmospheres, 97 (D9), 99199933, doi:10.1029/92jd00719, 1992.
771 Rogers, R. F., Fritsch, J. M., and Lambert, W. C.: A simple technique for using radar data in the dynamic
772 initialization of a mesoscale model, Mon. Weather Rev., 128, 2560–2574, 2000.
773 Romps, D. M., Seeley, J. T., Vollaro, D., and Molinari, J.: Projected increase in lightning strikes in the
774 United States due to global warming, Science, 346 (6211), 851854, doi:10.1126/science.1259100,
775 2014.
776 Rudlosky, S. D., and Shea, D. T.: Evaluation WWLLN performance relative to TRMM/LIS, Geophys.
777 Res. Lett., 40, 2344-2348, doi:10.1002/grl.50428, 2013.
778 Sims, A. P., Alapaty, K., and Raman, S.: Sensitivities of Summertime Mesoscale Circulations in the
779 Coastal Carolinas to Modifications of the Kain-Fritsch Cumulus Parameterization, Mon. Wea. Rev.,
780 145, 4381-4399, doi:10.1175/MWR-D-16-0047.1, 2017.
781 Skamarock, W. C., and Klemp, J. B.: A time-split nonhydrostatic atmospheric model, Journal of
782 Computational Physics, 227, 3465-3485, doi:10.1016/j.jcp.2007.01.037, 2008.
783 Stolzenburg, M., and Marshall, T. C.: Electric field and charge structure in lightning-producing clouds,
784 Lightning: Principles, Instruments and Applications, H.-D. Betz, U. Schumann, P. Laroche (Eds.),
785 641 pp., Springer, doi:10.1007/978-1-4020-9079-0_3, 2009.
786 U.S. EPA: Meteorological Model Performance for Annual 2016 Simulation WRF v3.8, EPA-454/R-19-
787 010, https://www.epa.gov/sites/default/files/2020-10/documents/met_model_performance-
788 2016_wrf.pdf, 2019.
789 Zheng, Y., Alapaty, K., Herwehe, J. A., Del Genio, A. D., and Niyogi, D.: Improving high-
790 resolution weather forecasts using the Weather Research and Forecasting (WRF) Model with

an updated Kain–Fritsch scheme, Mon. Wea. Rev., 144, 833–860, doi:10.1175/MWR-D-15-0005.1, 2016.

Table 1. Model Cases used in this study. The case names are comprised of elements from the other four columns, which describe the simulation domain (blank = CONUS, H = hemispheric), the version of the Kain-Fritsch trigger that was applied (trigger 1 = K1, trigger 2 = K2), the frequency that the convective properties was updated (every time step = C0, every 10 minutes = C10), and the lightning data that were assimilated in the simulation (B = Base/none, N = NLDN, W = WWLLN).

Case Name	Domain (none or H)	trigger (K1 or K2)	cudt (C0 or C10)	LTA Network (B, N, W)
K1C0B	CONUS	1	0	Base/none
K1C10B	CONUS	1	10	Base/none
K2C0B	CONUS	2	0	Base/none
K2C10B	CONUS	2	10	Base/none
K1C0N	CONUS	1	0	NLDN
K1C10N	CONUS	1	10	NLDN
K2C0N	CONUS	2	0	NLDN
K2C10N	CONUS	2	10	NLDN
K1C0W	CONUS	1	0	WWLLN
K1C10W	CONUS	1	10	WWLLN
K2C0W	CONUS	2	0	WWLLN
K2C10W	CONUS	2	10	WWLLN
HK1C0B	Hemisphere	1	0	Base/none
HK1C10B	Hemisphere	1	10	Base/none
HK2C0B	Hemisphere	2	0	Base/none
HK2C10B	Hemisphere	2	10	Base/none
HK1C0W	Hemisphere	1	0	WWLLN
HK1C10W	Hemisphere	1	10	WWLLN
HK2C0W	Hemisphere	2	0	WWLLN
HK2C10W	Hemisphere	2	10	WWLLN

803

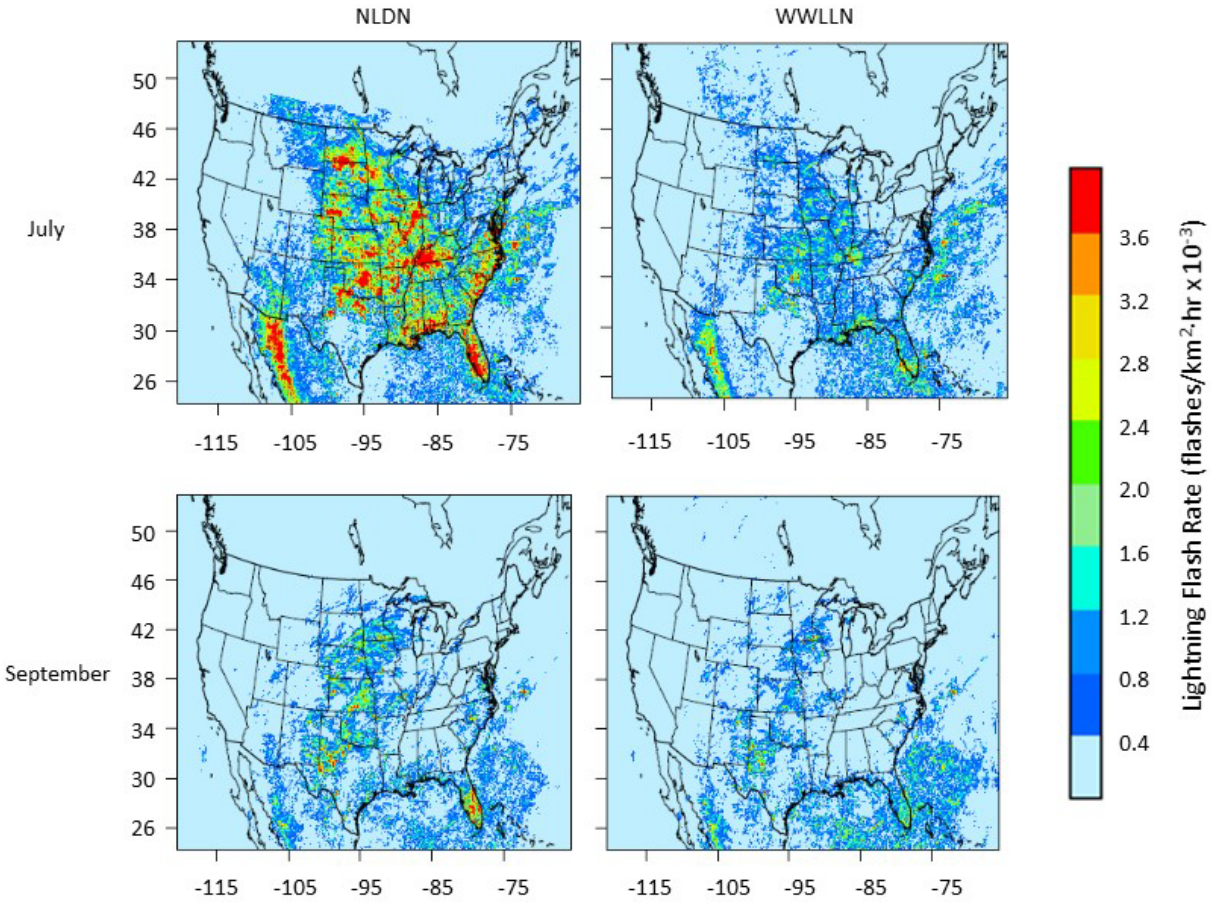

804

805 **Figure 1.** The mean hourly lightning flash rate from NLDN and WWLLN over the 12km

806 CONUS domain in July and September 2016.

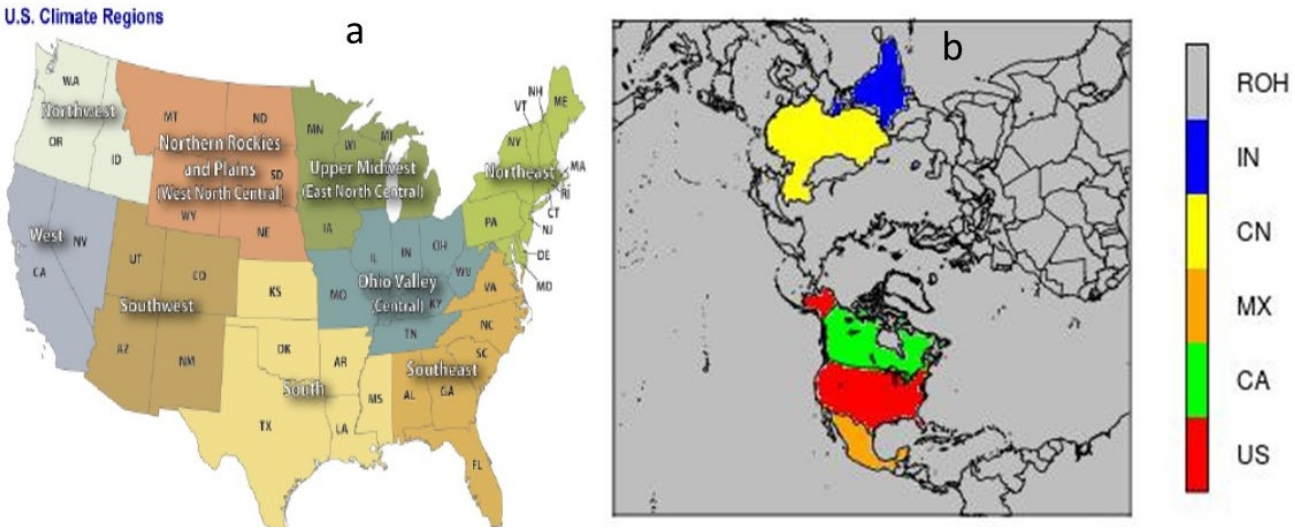

807

808 **Figure 2.** Analysis Regions (Countries), a. the climate regions in the CONUS, and b. the
809 countries over the northern hemisphere – US: United States; CA: Canada; MX: Mexico; CN:
810 China; IN: India; ROH: Other countries/regions except the five specific countries in the
811 hemispheric domain. The U.S. climate regions are: Northeast (NE), Southeast (SE), Ohio Valley
812 Central (OVC), Upper Midwest (UM), South, West North Central (WNC), Southwest (SW),
813 Northwest (NW), and West.

814

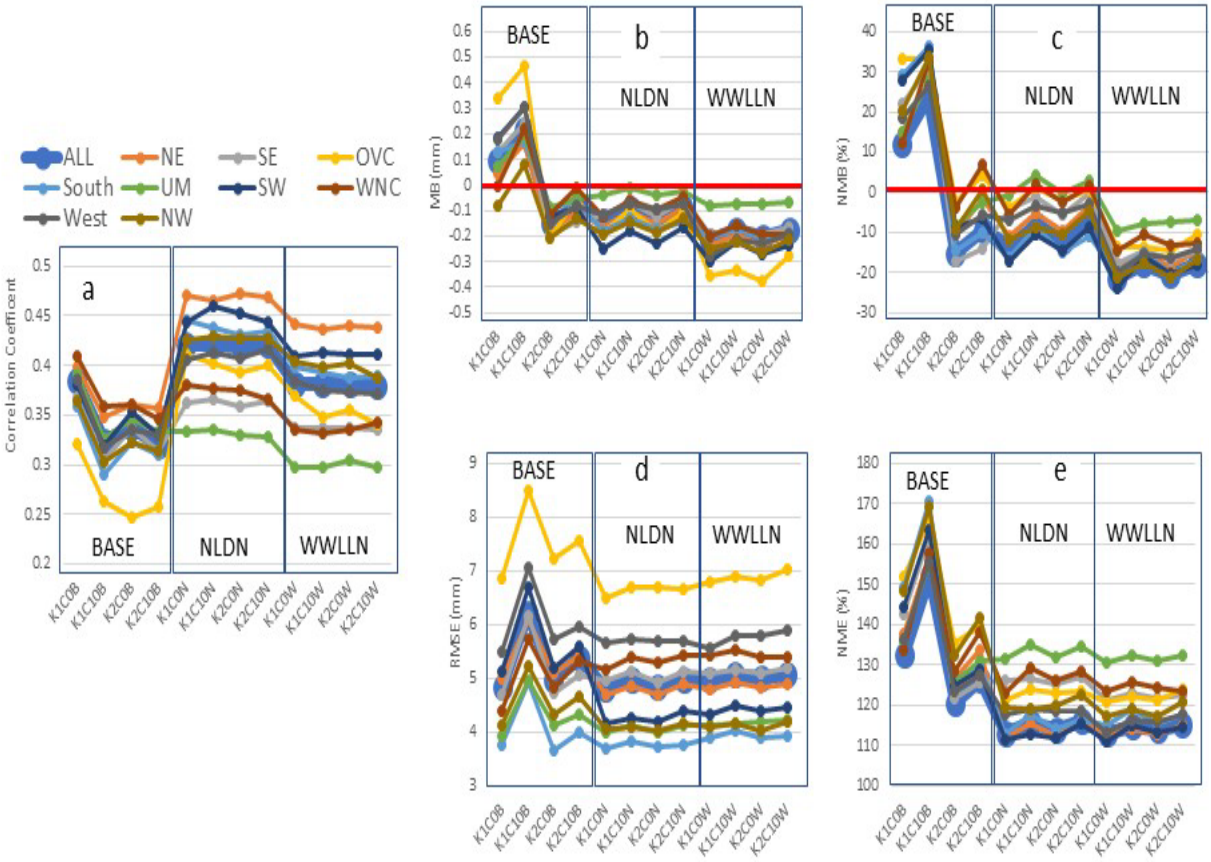

Figure 3. Monthly mean statistics for precipitation from BASE and LTA simulations comparing to the values from PRISM for the modeling domain and the climatological regions over the CONUS, respectively, during July 2016: a) correlation coefficient, b) MB, c) NMB, d) RMSE, and e) NME. In each plot, there are three sets of simulations (BASE, LTA with NLDN, and LTA with WWLLN) and each having four cases from the combinations of cumulus parameters.

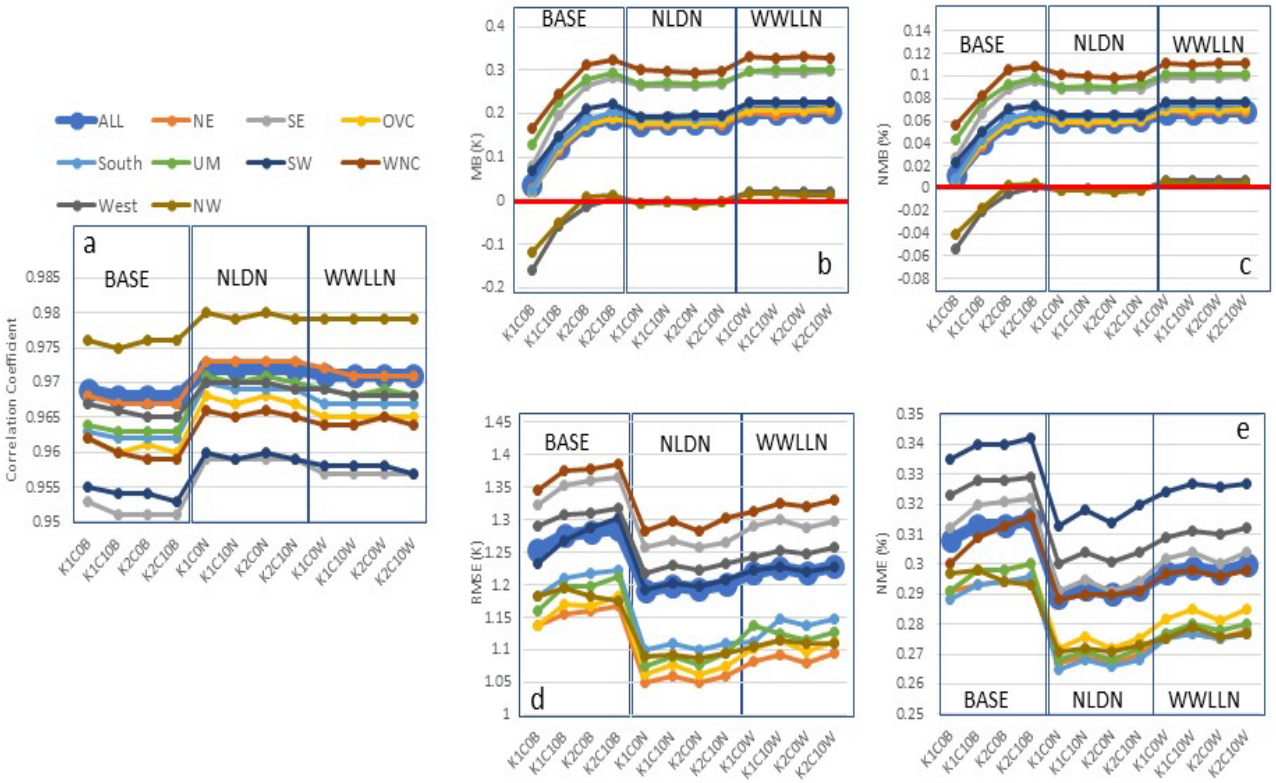

Figure 4. Same as Figure 3, but for 2-m temperature (T2) in that the simulated T2 values are paired with observations from NCEI's land-based stations in time and space (hourly mean values).

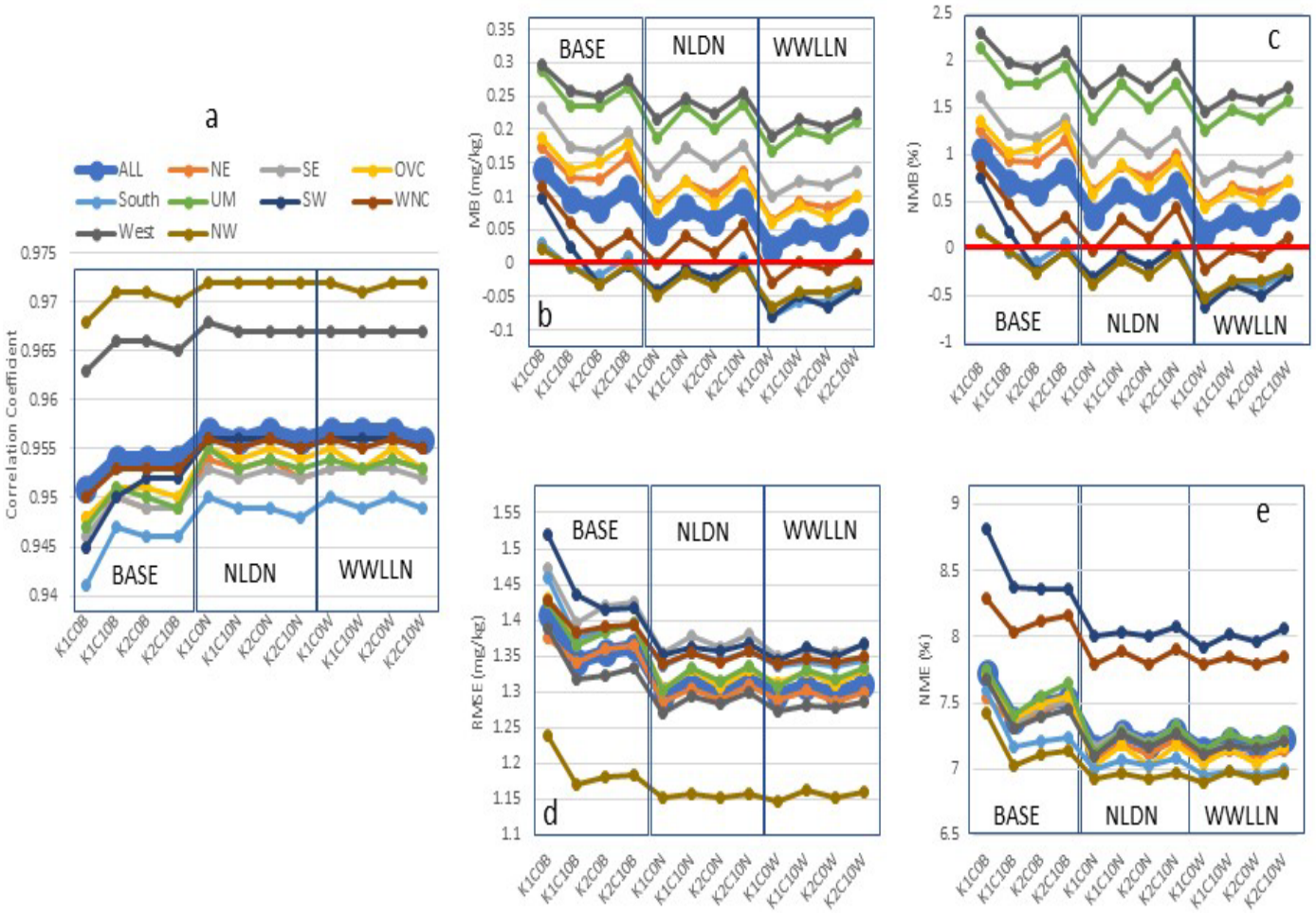

Figure 5. Same as Figure 4, but for 2-m water vapor mixing ratio.

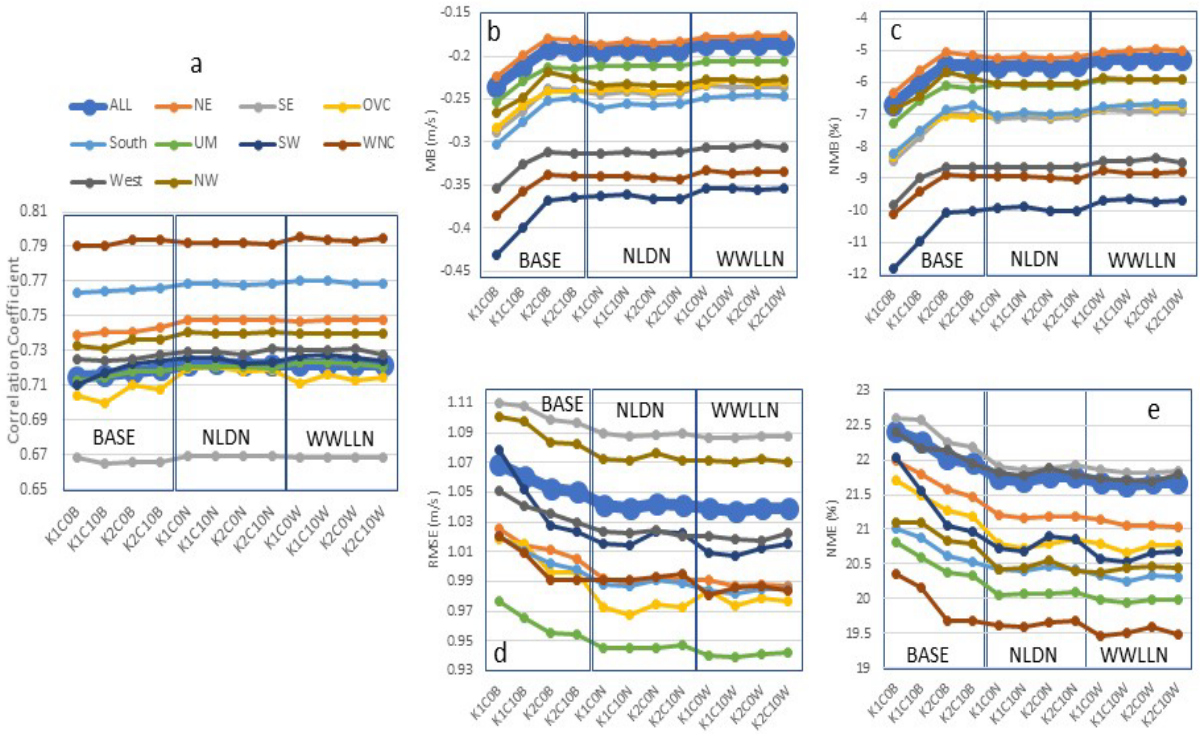

Figure 6. Same as Figure 4, but for 10-m wind speed.

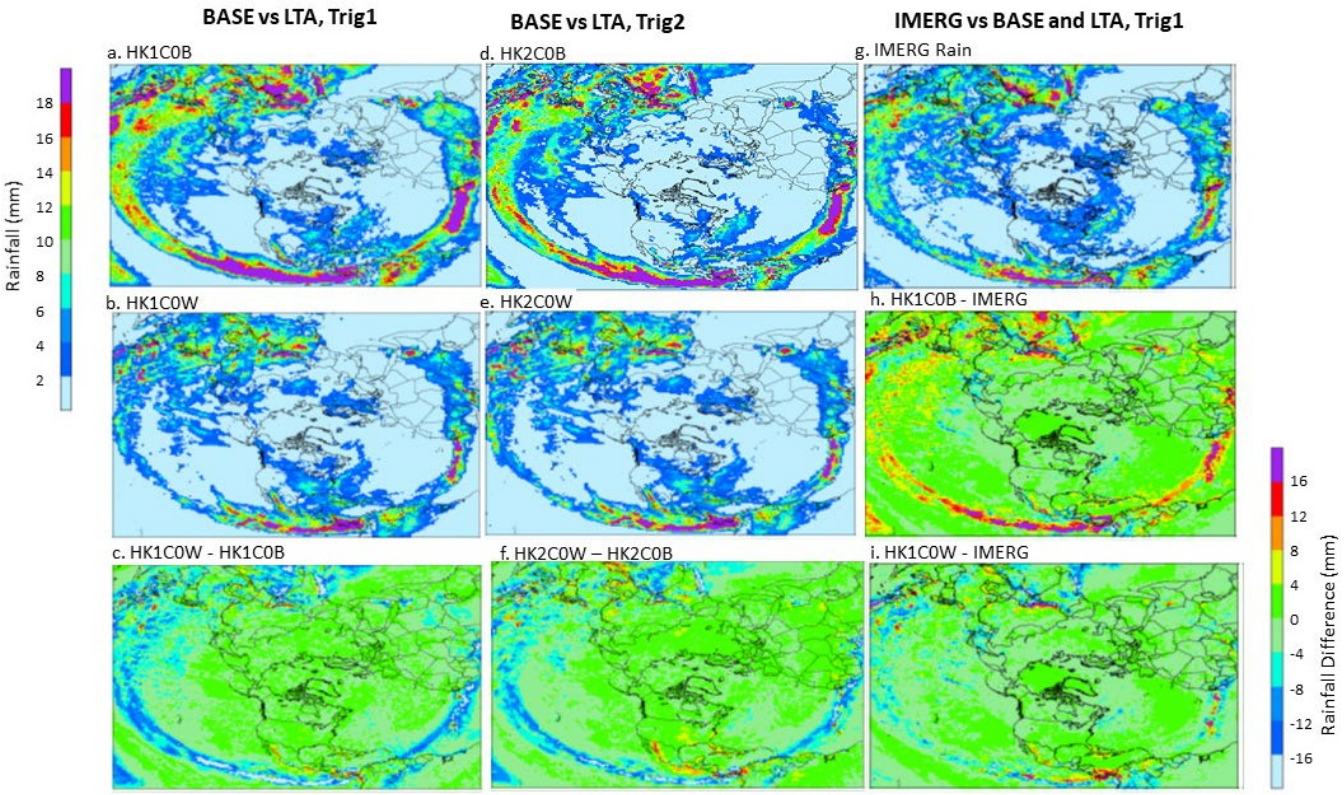

Figure 7. The mean daily rainfall during July 2016 simulated by base model cases (a. HK1C0B and d. HK2C0B), LTA cases (b. HK1C0W and e. HK2C0W), and the satellite GPM produced rainfall (g), and the differences between the LTA and BASE cases (c. HK1C0W – HK1C0B and f. HK2C0W – HK2C0B) and between the simulated cases and satellite IMERG products (h. HK1C0B – IMERG and i. HK1C0W – IMERG). Note that the left legend applies to the rain maps (a, b, d, e, and g), and the right legend applies to the difference plots (c, f, h, and i).

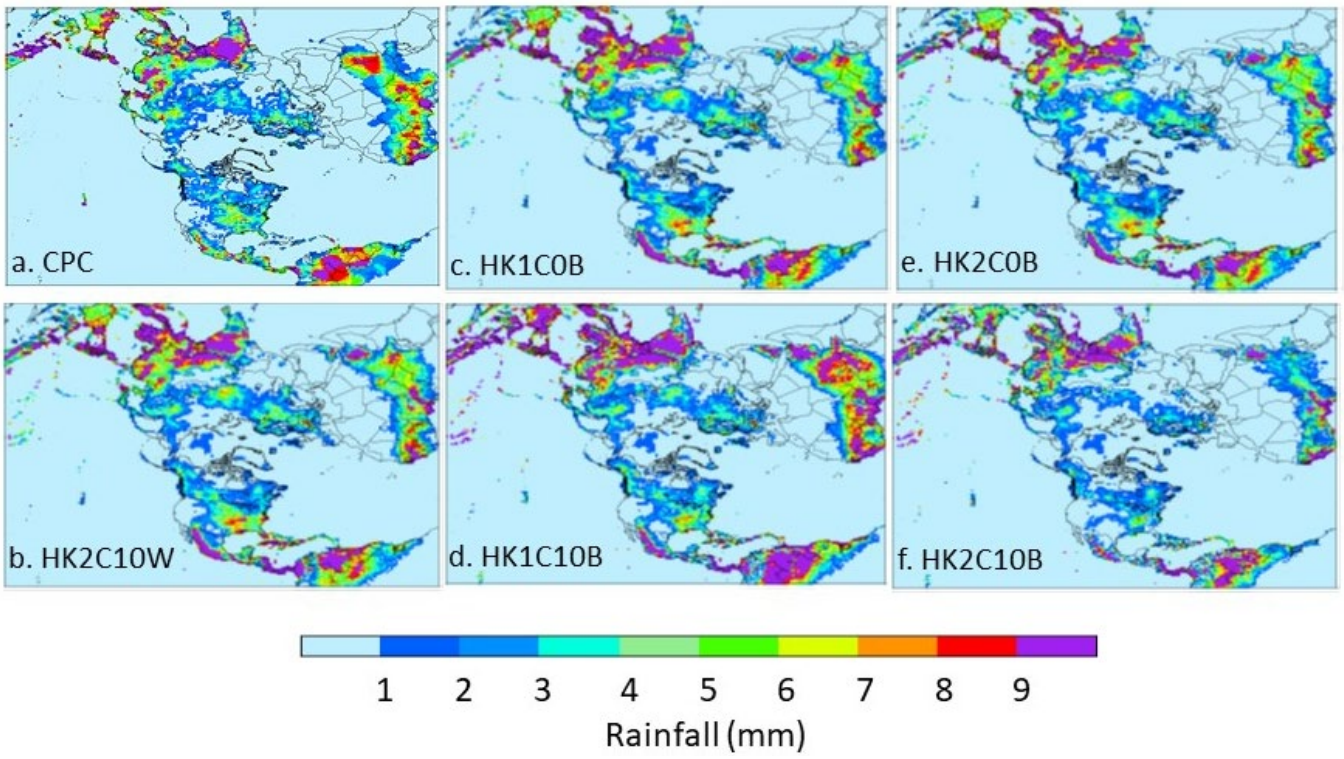

Figure 8. CPC rainfall (a) and simulated (b-f) mean daily precipitation during July 2016 over the hemispheric domain. The LTA configuration is represented by one case (b. HK2C10W) since all the LTA cases with different cumulus parameters produced similar results. All BASE cases are shown here (c-f) because the cumulus parameters do impact the simulated precipitation when not using LTA.

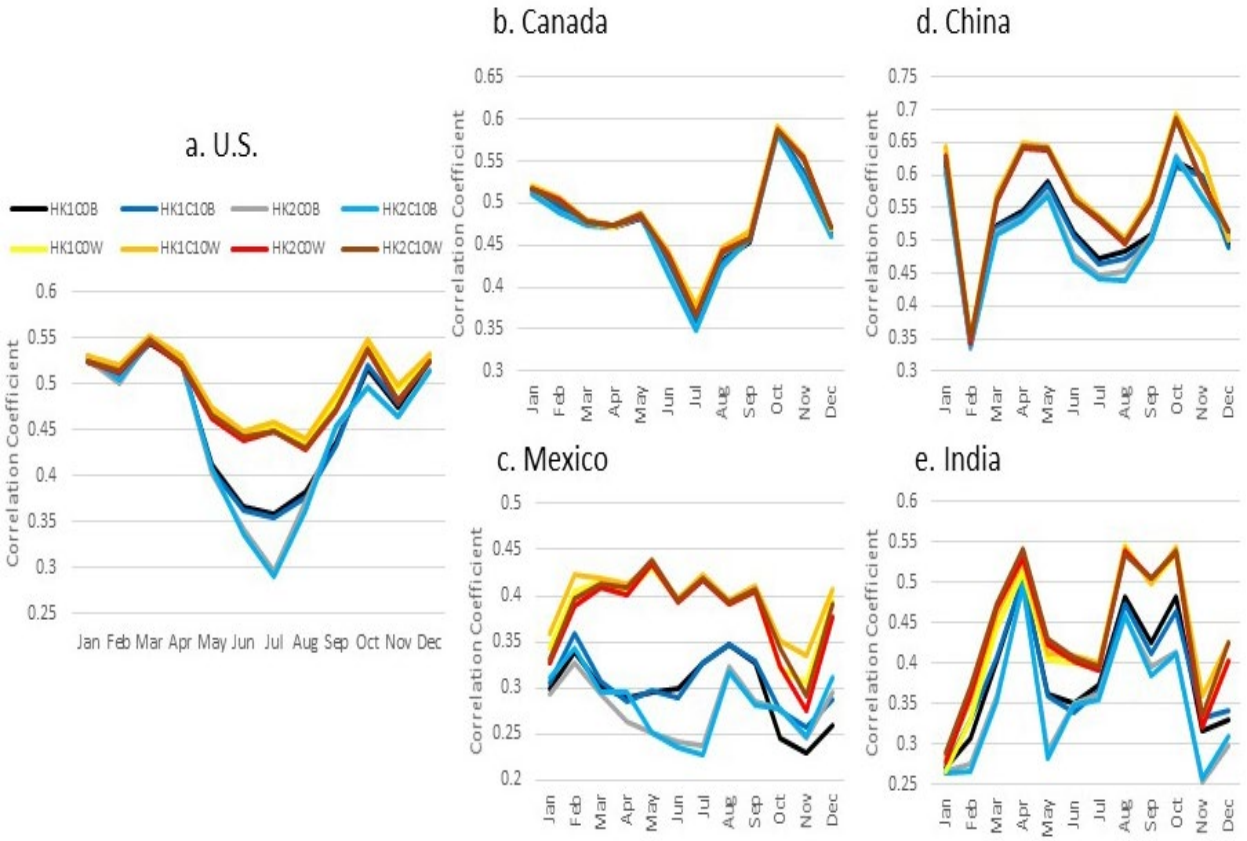

Figure 9. The monthly correlation coefficient between CPC and simulated precipitation in selected countries: a. United States, b. Canada, c. Mexico, d, China, and e. India. Note that all the BASE cases are plotted in cool colors and LTA cases in warm colors.

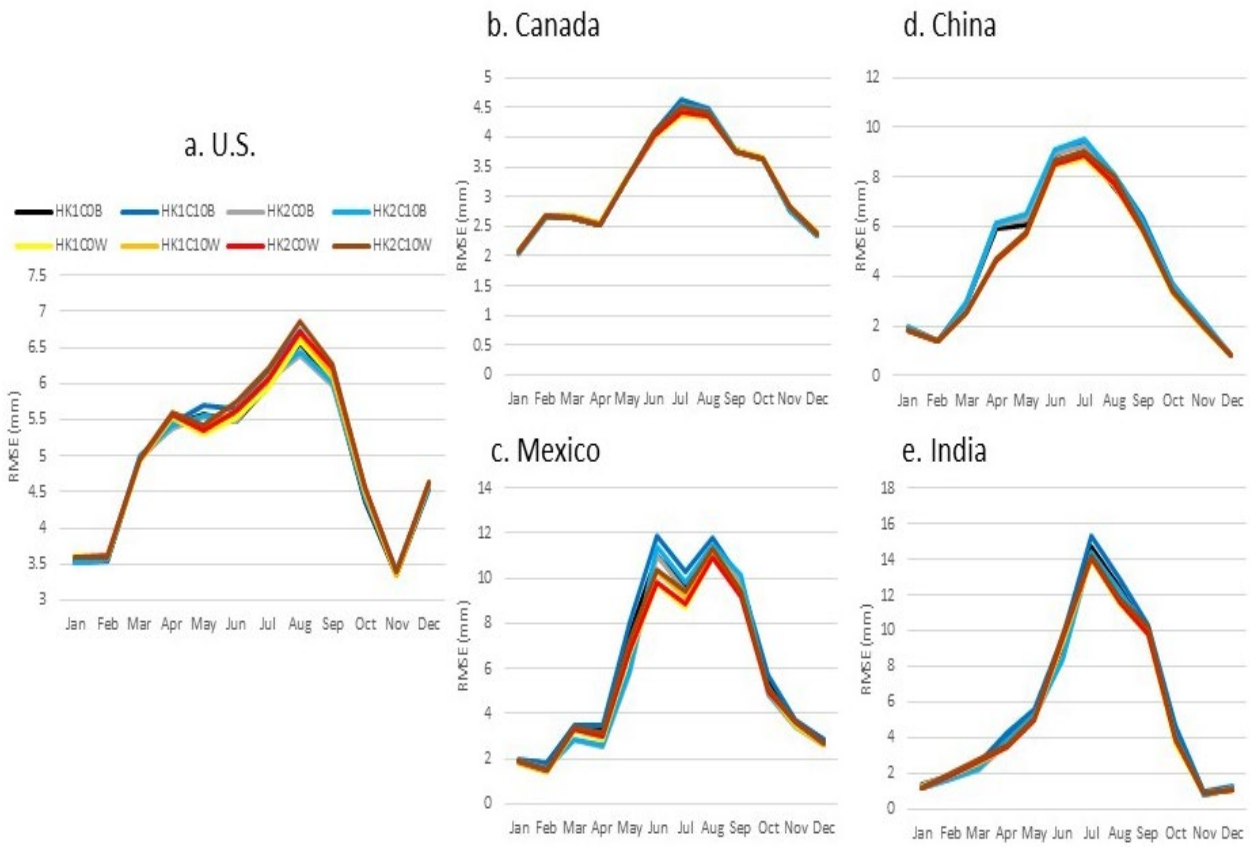

Figure 10. Same as Figure 9, but for RMSE.

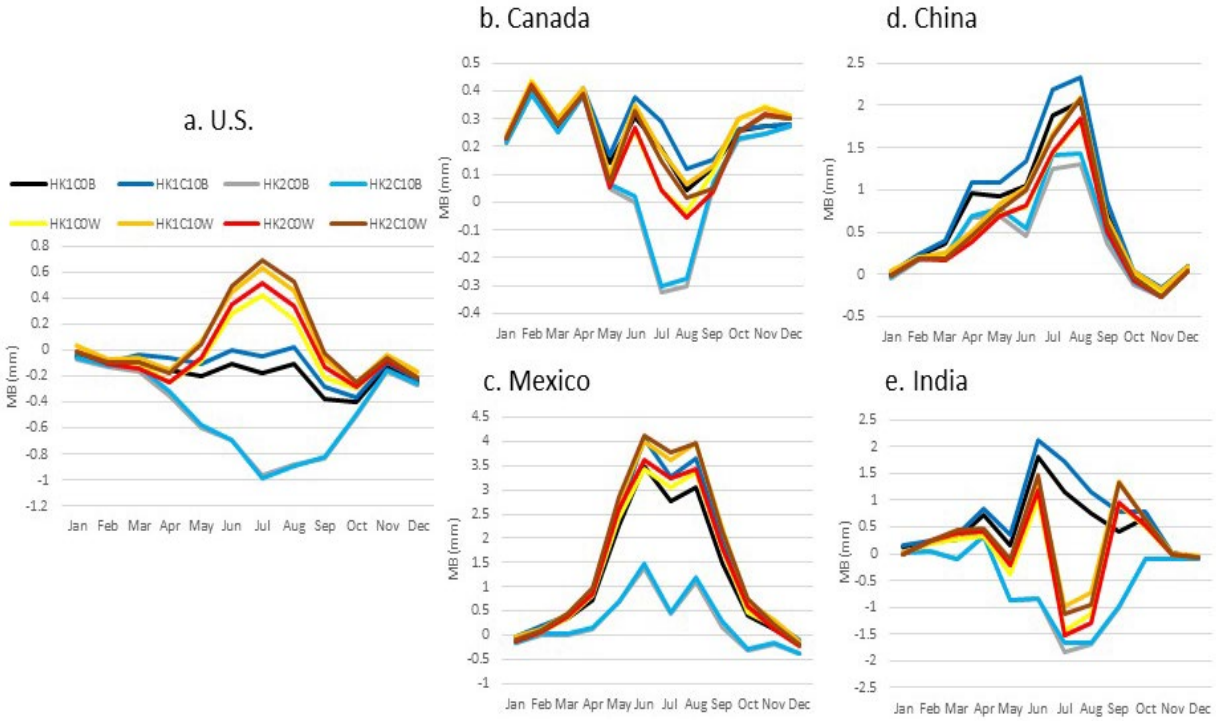

Figure 11. Same as Figure 9, but for MB.

872

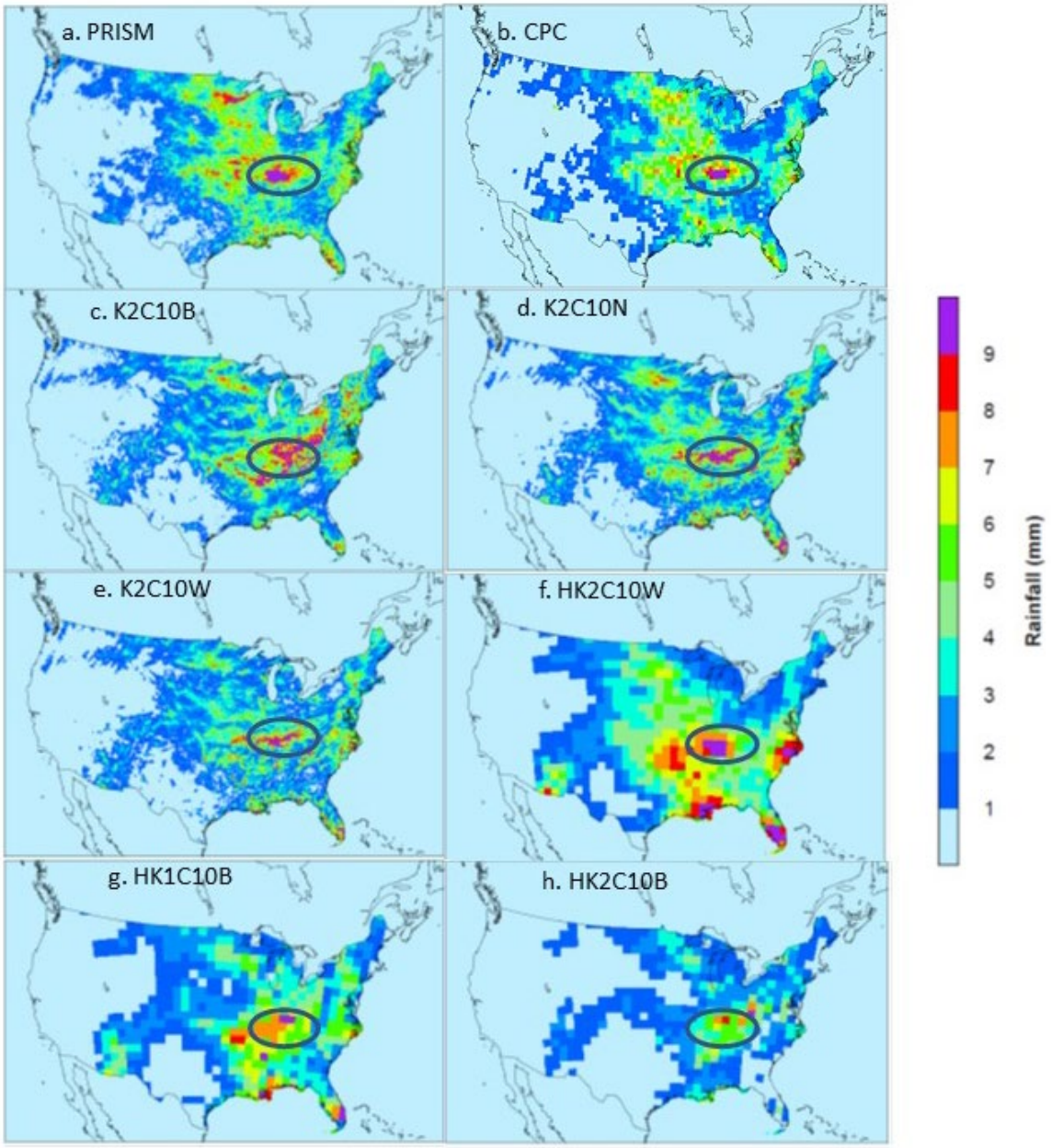

873

874 **Figure 12.** Mean daily precipitation over the CONUS during July 2016 from a) PRISM, b) CPC,
875 c) K2C10B, d) K2C10N, e) K2C10W, and f) HK2C10W, g) HK1C10B, and h)
876 HK2C10B. Note that all the observational based products and the 108 km hemispheric
877 simulations are regridded onto the 12 km CONUS domain.
878

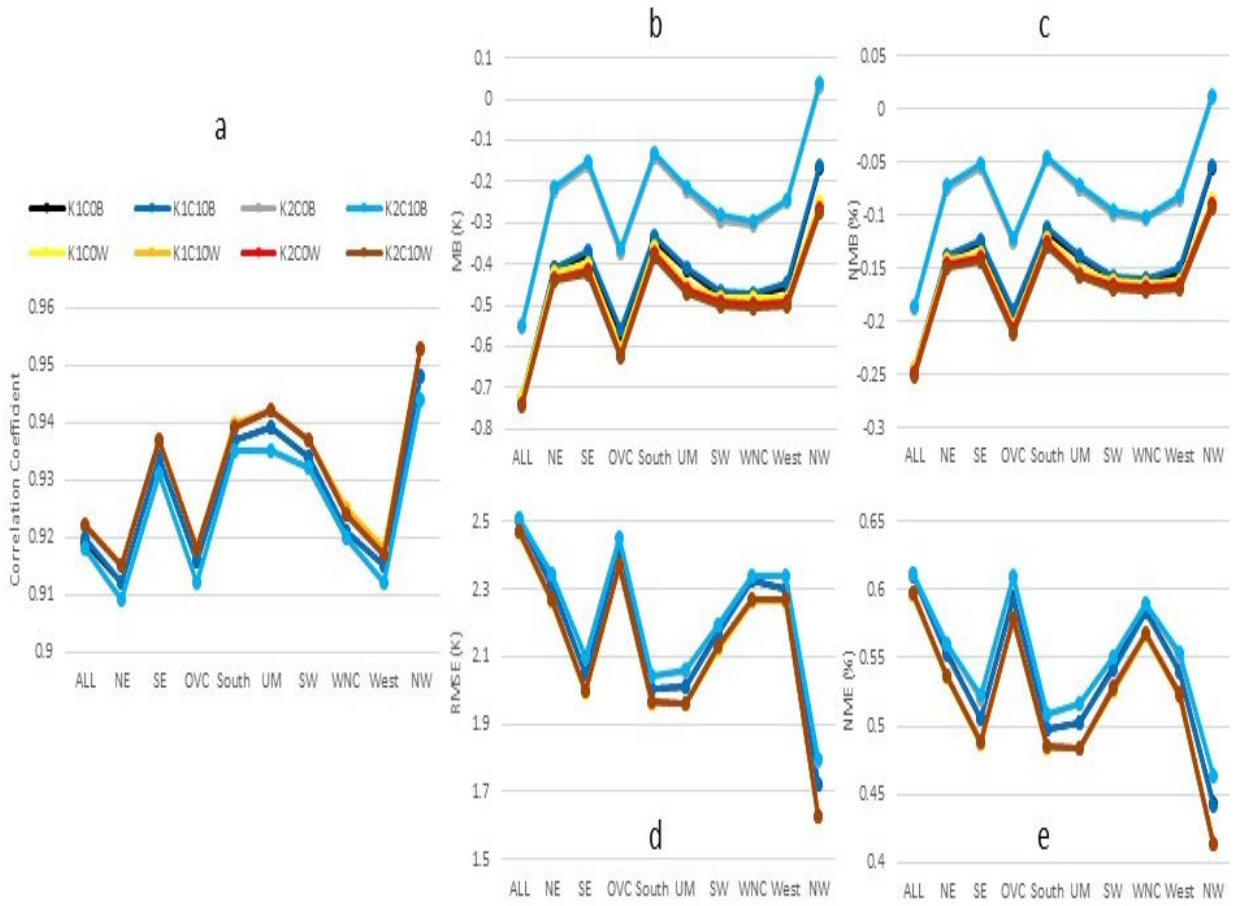

Figure 13. Monthly mean statistics for 2-m temperature from hemispheric BASE and LTA simulations comparing to surface observations during July 2016: a) correlation coefficient, b) MB, c) NMB, d) RMSE, and e) NME.

885

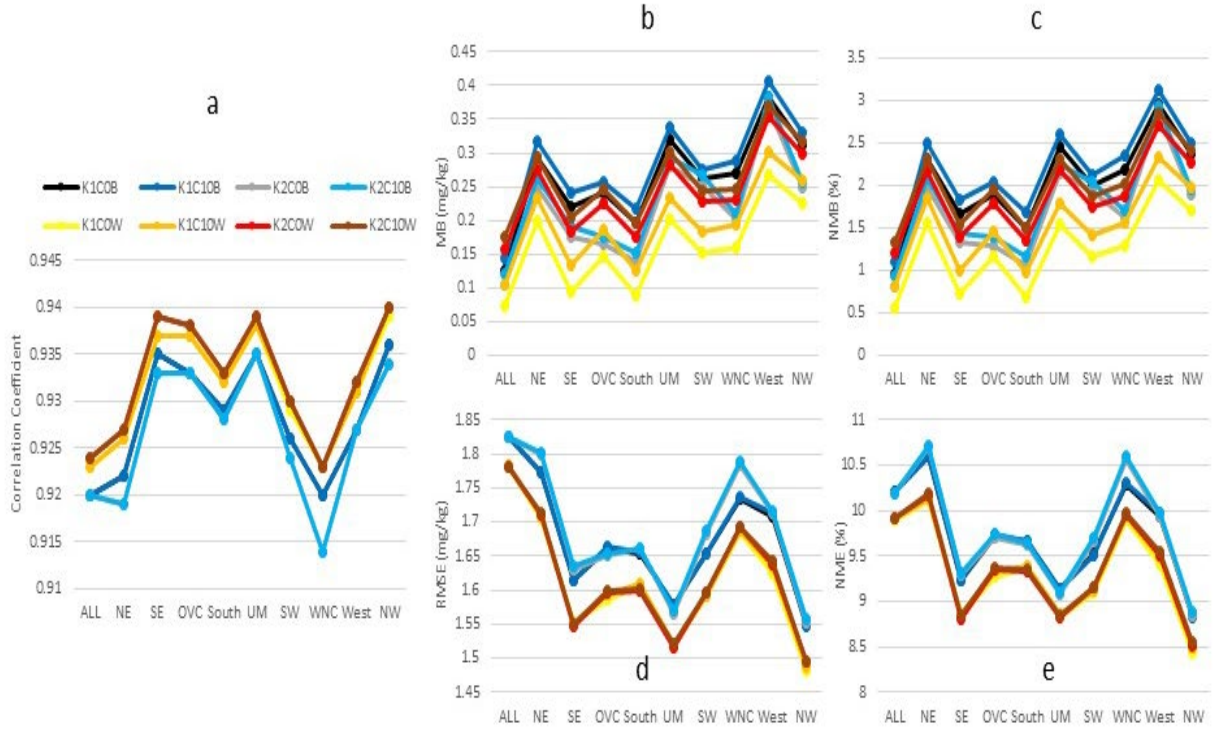

886

887 **Figure 14.** Same as Figure 12, but for 2-m water vapor mixing ratio.

888